Title

Copper(II) Binding to PBT2 Differs from That of Other 8-Hydroxyquinoline Chelators: Implications for the Treatment of Neurodegenerative Protein Misfolding Diseases

Journal

Inorganic Chemistry, 59(23)

ISSN

0020-1669

Authors

Summers, Kelly L
Roseman, Graham P
Sopasis, George J
et al.

Publication Date

2020-12-07

DOI

10.1021/acs.inorgchem.0c02754

Peer reviewed

HHS Public Access

Author manuscript

Inorg Chem. Author manuscript; available in PMC 2021 March 03.

Published in final edited form as:

Inorg Chem. 2020 December 07; 59(23): 17519–17534. doi:10.1021/acs.inorgchem.0c02754.

Copper(II) Binding to PBT2 Differs from That of Other 8-Hydroxyquinoline Chelators: Implications for the Treatment of Neurodegenerative Protein Misfolding Diseases

Kelly L. Summers,
Molecular and Environmental Sciences Group, Department of Geological Sciences and Department of Chemistry, University of Saskatchewan, Saskatoon, Saskatchewan S7N 5E2, Canada

Graham P. Roseman,
Department of Chemistry and Biochemistry, University of California, Santa Cruz, Santa Cruz, California 95064, United States

George J. Sopasis,
Department of Chemistry, University of Adelaide, South Australia 5005, Australia

Glenn L. Millhauser,
Department of Chemistry and Biochemistry, University of California, Santa Cruz, Santa Cruz, California 95064, United States

Hugh H. Harris,
Department of Chemistry, University of Adelaide, South Australia 5005, Australia

Ingrid J. Pickering,
Molecular and Environmental Sciences Group, Department of Geological Sciences and Department of Chemistry, University of Saskatchewan, Saskatoon, Saskatchewan S7N 5E2, Canada

Graham N. George
Molecular and Environmental Sciences Group, Department of Geological Sciences and Department of Chemistry, University of Saskatchewan, Saskatoon, Saskatchewan S7N 5E2, Canada

Corresponding Authors: Kelly L. Summers – Molecular and Environmental Sciences Group, Department of Geological Sciences and Department of Chemistry, University of Saskatchewan, Saskatoon, Saskatchewan S7N 5E2, Canada; kelly.summers@usask.ca; Ingrid J. Pickering – Molecular and Environmental Sciences Group, Department of Geological Sciences and Department of Chemistry, University of Saskatchewan, Saskatoon, Saskatchewan S7N 5E2, Canada; ingrid.pickering@usask.ca; Graham N. George – Molecular and Environmental Sciences Group, Department of Geological Sciences and Department of Chemistry, University of Saskatchewan, Saskatoon, Saskatchewan S7N 5E2, Canada; g.george@usask.ca.

Supporting Information

The Supporting Information is available free of charge at https://pubs.acs.org/doi/10.1021/acs.inorgchem.0c02754.
Calculated log *P* values; UV–visible absorption spectra; additional information on density functional theory calculations; comparison of HERFD-XAS and conventional XAS near edges; additional XAS near-edge spectra of a titration of Cu(II) and PBT2; diagrams of multiple scattering angles; calculated multiple scattering angles for Cu(II)-*bis*-PBT2 complexes; alternative EXAFS fitting results; and EXAFS fitting parameters (PDF)

Complete contact information is available at: https://pubs.acs.org/10.1021/acs.inorgchem.0c02754

The authors declare no competing financial interest.

Abstract

PBT2 (5,7-dichloro-2-[(dimethylamino)methyl]-8-hydroxyquinoline) is a small Cu(II)-binding drug that has been investigated in the treatment of neurodegenerative diseases, namely, Alzheimer's disease (AD). PBT2 is thought to be highly effective at crossing the blood–brain barrier and has been proposed to exert anti-Alzheimer's effects through the modulation of metal ion concentrations in the brain, specifically the sequestration of Cu(II) from amyloid plaques. However, despite promising initial results in animal models and in clinical trials where PBT2 was shown to improve cognitive function, larger-scale clinical trials did not find PBT2 to have a significant effect on the amyloid plaque burden compared with controls. We propose that the results of these clinical trials likely point to a more complex mechanism of action for PBT2 other than simple Cu(II) sequestration. To this end, herein we have investigated the solution chemistry of Cu(II) coordination by PBT2 primarily using X-ray absorption spectroscopy (XAS), high-energy-resolution fluorescence-detected XAS, and electron paramagnetic resonance. We propose that a novel *bis*-PBT2 Cu(II) complex with asymmetric coordination may coexist in solution with a symmetric four-coordinate Cu(II)-*bis*-PBT2 complex distorted from coplanarity. Additionally, PBT2 is a more flexible ligand than other 8HQs because it can act as both a bidentate and a tridentate ligand as well as coordinate Cu(II) in both 1:1 and 2:1 PBT2/Cu(II) complexes.

Graphical Abstract

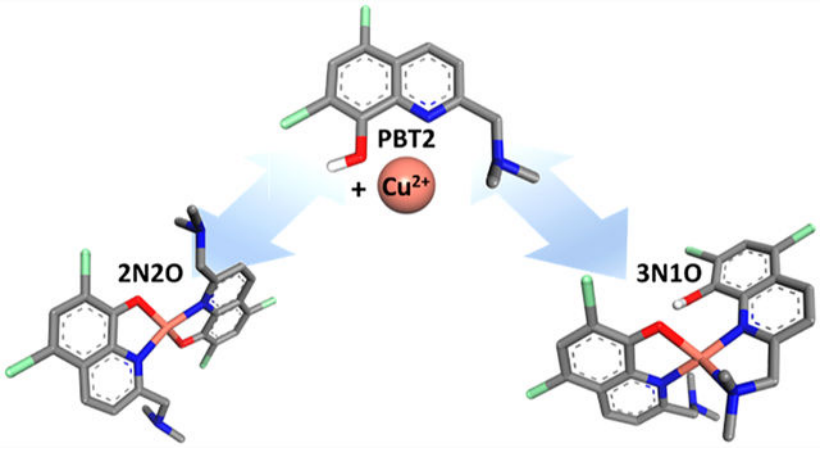

1. INTRODUCTION

PBT2 (5,7-dichloro-2-[(dimethylamino)methyl]-8-hydroxyquinoline) was designed as a second-generation metal-protein-attenuating compound for the treatment of Alzheimer's disease (AD), following difficulties in synthesizing PBT1 (5-chloro-7-iodo-8-hydroxyquinoline; clioquinol; CQ). In designing potential drugs for neurological diseases, small hydrophobic compounds with metal-binding ligands are thought to be effective at crossing the blood–brain barrier and restoring metal ion homeostasis within the brain. Two such effective drug compounds, CQ and PBT2 (Figure 1), have been the focus of clinical trials for the treatment of AD and have been shown to significantly improve cognition in both animal models[1,2] and AD patients.[3–6]

Because CQ had previously been linked to the outbreak of subacute myelo-optic neuropathy (SMON), clinical trials to test the compound as an AD therapeutic proceeded cautiously with controlled dosing. Between 1955 and 1970, more than 10 000 SMON cases were reported in Japan, with symptoms including blindness, lower limb spasticity, and sensory dysfunction;[7,8] many people were permanently disabled.[7] The exact cause of SMON is still debated; however, excessive consumption of CQ[8] (up to 4 g/day in one case[9]) is thought to induce a severe deficiency in essential metals such as copper, zinc, and iron.[10–14] Despite concerns surrounding the safety of CQ, no adverse effects of CQ or PBT2 treatment were reported in animals given 30 mg/kg/day orally or in patients in preclinical or clinical studies given up to 750 mg/day orally for the treatment of AD.[1–3,5,6]

Preclinical studies of CQ in Alzheimer's model mice showed promising results, including decreased amyloid plaque burden and improved memory.[1,2] Similarly, improvements in memory and cognition were reported from a phase II clinical trial[3] and a case study[4] on CQ in AD patients. Despite promising results from clinical trials investigating CQ, the contamination of large-scale synthesis halted further testing of this drug as an effective AD treatment.[2] The results of the clinical trial of PBT2 in 2014 are yet to be published in a peer-reviewed scientific journal; however, PBT2 was reported to have no significant effect on the amyloid burden[15,16] despite previously observed improvements in cognitive function.[2,5] More recent analyses propose that PBT2 may reduce the levels of phosphorylated-τ aggregates and thereby improve neuronal survival,[17–19] suggesting that PBT2 has the potential to target both proteins at the root of Alzheimer's: amyloid beta (Aβ) and τ.

In addition to AD, phosphorylated-τ also plays a role in other neurodegenerative disorders, such as Parkinson's disease and possibly Huntington's disease. PBT2 and CQ were also evaluated for the treatment of Huntington's disease (HD). Studies of CQ in animal models of HD noted improved behavioral and pathologic phenotypes, including decreased huntingtin aggregate accumulation.[20] CQ was abandoned as a potential treatment in HD, as it was in AD, because of the difficulties associated with large-scale synthesis. However, PBT2 was subsequently tested in animal models of HD and was found to have similar positive outcomes to its predecessor.[21] In addition, PBT2 was shown to improve cognition, particularly executive function, and to reduce brain atrophy in HD clinical trials.[18,19,22] PBT2 is presumed to act by inhibiting the interaction between the HD-causing huntingtin protein and copper in the brain, similar to CQ.[20]

Although these chelators have been postulated to restore metal ion homeostasis, with copper and zinc redistribution into deficient neurons thought to trigger a signaling cascade that results in reduced amyloid β levels in the brain and improved cognition,[23,24] questions surrounding their mechanism of action remain. The results of the above-mentioned studies investigating the efficacy of CQ and PBT2 in the treatment of neurodegenerative diseases of protein misfolding would appear to point to a more complex mechanism of action for these drugs and would seem to suggest that more information should be acquired before they are completely discounted as a treatment. It is likely that the behavior of PBT2 is related to its metal-binding capacity and the structure(s) of the resultant metal-bound PBT2 complex(es).

We have previously investigated the solution structures of Cu(II) complexes with other 8-hydroxyquinolines (8HQs) using X-ray absorption spectroscopy (XAS) and high-energy-resolution fluorescence-detected X-ray absorption spectroscopy (HERFD) XAS.[25,26] Structures of other Cu(II) complexes with 8HQ-based ligands have also been investigated previously by other groups.[27–30] The chemical identity of PBT2 was released in 2014 (patented by Prana Biotechnology Ltd.); structural studies have therefore been limited until relatively recently. However, Kenche et al.[27] investigated the solution structure of a similar 8HQ compound without chlorine substituents, 2-[(dimethylamino)methyl]-8-hydroxyquinoline, using electron paramagnetic resonance (EPR) and UV–visible absorption spectroscopy along with geometry optimization calculations to propose two possible structures for this ligand, dependent on solution conditions. One structure depicted a tridentate 8HQ ligand coordinating Cu(II), along with an exchangeable Cl^- ligand, in an approximately square-planar environment. The other structure was that of a pentacoordinate Cu(II)-*bis*-8HQ complex with participation from the tertiary amine in only one of the two 8HQ moieties. Although chlorine substituents on the 8HQ moiety have been shown to affect the hydrophobicity of the compound,[31] it is unclear what effect these substituents may have on Cu(II) coordination. In a more recent study by Nguyen et al.,[29] three Zn(II)-PBT2 crystal structures, one Cu(II)-*bis*-PBT2 crystal structure, and three additional calculated structures for Cu(II)-*mono*-PBT2 were described.

To better understand the aqueous solution chemistry of PBT2, we investigated the structure of Cu(II) complexes with PBT2 using a combination of conventional spectroscopies, including EPR and UV–visible absorption, as well as synchrotron XAS and HERFD XAS. To circumvent the known solubility issues with 8-hydroxyquinoline compounds and their complexes with Cu(II) and to avoid the use of organic solvents, we have again used a buffer system that includes a surfactant to allow us to probe the Cu(II) PBT2 complex(es) in aqueous solution at physiological pH.[26] We show that PBT2 binds Cu(II) in a different coordination environment from that of other 8HQs in solution.[26] Specifically, our HERFD-XAS results show a split 1s → 3d near-edge transition, which is likely to indicate a mixture of Cu(II) species, as it is difficult to reconcile multiple peaks with a single chemical entity. On the basis of our EPR and XAS data, in solutions containing excess PBT2, a Cu(II)-*bis*-PBT2 complex is likely the preferred structure, whereas in solutions of equimolar PBT2 and Cu(II) there is a mixture of species. On the basis of the results from EPR, it is clear that a minimum of three species exist in equimolar solutions.

2. RESULTS AND DISCUSSION

8-Hydroxyquinoline compounds, and particularly their Cu(II) complexes, are hydrophobic, resulting in a number of solubility issues, namely, precipitate formation, in many previous studies on PBT2[29,32] and other 8HQs.[31,33–37] As a result of this low solubility, nearly all experimental work reported to date on such complexes has used powders, crystals, or abiological solvents such as dimethyl sulfoxide (DMSO), dimethylformamide (DMF), or toluene. We previously devised a buffer system that includes a surfactant (dodecyl trimethylammonium bromide (DTAB) in 3-(*N*-morpholino)propanesulfonic acid (MOPS)) to allow us to probe Cu(II) 8HQ complexes in aqueous solution at physiological pH.[26] Our buffered surfactant solution is closer to a true aqueous solution, which is the goal in studying

systems with biological applications. The use of surfactant also allowed us to avoid the use of cryoprotectants such as glycerol in our XAS studies; this is advantageous in avoiding beam-induced photodamage.[38]

2.1. EPR of Cu(II) PBT2 Complexes.

The EPR spectra of Cu(II) complexes with PBT2 (Figure 2) are different than those published previously for other 8HQs.[25,26,32] Specifically, EPR spectra of Cu(II) PBT2 lack the striking nitrogen hyperfine structure in spectra of both coplanar Cu(II)-*bis*-8HQ and distorted 2-position-substituted 2-methyl-8HQ.[26] EPR spectra of Cu(II)-PBT2 made with $^{63}CuCl_2$ in 400 mM DTAB buffered with 100 mM MOPS at pH 7.4 have some similarities to the Cu(II) titration spectra published by Nguyen et al.[29] for PBT2 in DMSO and the 1:1 Cu(II)/PBT2 spectrum recently published by Sgarlata et al.[32] in aqueous solution at approximately pH 6.5. The spectrum of excess PBT2 to Cu(II) is magnetically dilute and consistent with a single species in solution (labeled component *i*; Figure 2b), which appears to disagree with reports by Kenche et al. on a similar 8HQ.[27] Conversely, the 1:1 Cu(II)/PBT2 spectrum appears to be a mixture of at least three species (labeled components *i*, *ii*, and *iii* in Figure 2d and e), in apparent agreement with previous results using PBT2 and other similar 8HQs.[27,29,32] The 1:1 Cu(II)/PBT2 spectrum initially appears to consist of at least two species that are likely present in approximately equal abundance; however, the difference spectrum that results from the subtraction of the excess PBT2 to Cu(II) spectrum from the 1:1 Cu(II)/PBT2 spectrum suggests that there is still a mixture of two species remaining (components *ii* and *iii*). Taking the double integral, which is proportional to the number of Cu(II) spins in the sample, of the initial 1:1 Cu(II)/PBT2 spectrum and comparing it with the double integral of the difference spectrum suggests that ~44% of the Cu(II) in this mixture can be attributed to the structure formed in the excess PBT2 with Cu(II) sample (i.e., component *i* in Figure 2). In the 1:2 Cu(II)/PBT2 spectrum (Figure 2c), there is still some component *ii* present but the solution mainly consists of component *i*.

Several species, in addition to the Cu(II)-*bis*-PBT2 complex, might be proposed to exist in the 1:1 Cu(II)/PBT2 solution, some of which have been proposed by Nguyen et al.[29] PBT2 has been proposed to show tridentate chelation of Cu(II) and therefore might require only one additional water or Cl^- ligand to form a Cu(II)PBT2 complex (Figure 3). Additionally, bidentate chelation of Cu(II) by PBT2 has not been ruled out and may be more favorable under some conditions (e.g., higher ratios of PBT2/Cu(II)) because of the strain imposed by the two adjacent five-membered chelate rings formed upon Cu(II) coordination in the tridentate complex. Therefore, complexes with PBT2 and two water ligands, two Cl^- ligands, or a mixture of water and Cl^- ligands may also be possible (Figure 3). Additionally, there is likely some Cu(II) in solution not bound by PBT2. A mixture of these species in solution might provide an explanation for the two components (i.e., components *ii* and *iii*) remaining in the difference spectrum in Figure 2e.

The second derivative of the excess PBT2 with Cu(II) EPR spectrum is shown in Figure 2a. The second derivative spectrum was simulated using significant g and A strains (Figure 2a), suggesting that this Cu(II) site has low symmetry. The five-line pattern in the A region of the second derivative is consistent with two approximately equivalent nitrogens bound to the

Cu(II) with a coupling of 20.2 MHz and was not fit well without including nitrogen hyperfine structure in the fit parameters. Previously, spectra of the coplanar Cu(II)-*bis*-8HQ and the distorted 2-CH_3-substituted Cu(II)-*bis*-M8Q complex showed prominent nitrogen hyperfine structure from approximately equivalent nitrogen ligands with hyperfine coupling values of 15.3 and 14.0 MHz, respectively.[26] In spectra of Cu(II)-*bis*-PBT2, nitrogen hyperfine splitting is visible only in the second derivative and has a larger coupling. This result suggests that the Cu(II) coordination environment in the Cu(II)-PBT2 complex has lower symmetry than that found previously for 2-CH_3-substituted 8HQs. Specifically, the broad nitrogen hyperfine splitting is consistent with Cu–N bond distances that are nonequivalent or with nitrogens in the N–Cu(II)–N that are not colinear.

EPR spectra were simulated to generate the g and A values listed in Table 1, and the simulated spectra are shown in Figure 2a and b. The spectra of Cu(II)-*bis*-PBT2 were best simulated by rhombic g values (where $g_x \neq g_y \neq g_z$), similar to EPR spectra of Cu(II)-*bis*-8HQ and -M8Q described previously[26] but in contrast to previous EPR investigations of Cu(II) 8HQ complexes which assumed axial symmetry. An anisotropic rhombic g tensor with $g_x \neq g_y$ is expected because these complexes do not possess true axial symmetry even in the coplanar Cu(II)-*bis*-8HQ complexes. Although similar g and A values were obtained by Sgarlata et al. and were proposed to indicate a square-based pyramidal geometry, we find little evidence to support this claim. EPR parameters determined herein appear to be more consistent with a four-coordinate environment with oxygen and nitrogen ligands, possibly 2 N 2 O or 3 N 1 O coordination, following the works of Peisach and Blumberg.[39] DFT calculations of EPR parameters for a 2 N 2 O coordination environment for Cu(II)-*bis*-PBT2 predict rhombic g values, specifically, $g_x = 2.047$, $g_y = 2.090$, and $g_z = 2.208$. Calculations for a 3 N 1 O coordination environment in the Cu(II)-*bis*-PBT2 complex (structure detailed below) also suggest rhombic g values, specifically, $g_x = 2.005$, $g_y = 2.169$, and $g_z = 2.206$. These calculated EPR parameters may indicate that the experimental EPR spectra are more consistent with a 2 N 2 O coordination environment for the Cu(II)-*bis*-PBT2 complex. The DFT-calculated N hyperfine couplings for both the 2 N 2 O and 3 N 1 O structures also give rhombic A (^{14}N) values. The pyridine nitrogens of the 2 N 2 O complex are predicted to have A_z (^{14}N) values of 36.1 MHz, whereas the pyridine nitrogens of the 3 N 1 O complex have calculated A_z (^{14}N) values of 32.6 and 30.5 MHz. The additional amino nitrogen ligand in the 3 N 1 O complex also has a predicted A_z (^{14}N) value of 35.7 MHz, highlighting the asymmetry of this complex.

2.2. XAS and HERFD-XAS Near-Edge Spectra of PBT2.

HERFD-XAS measures the X-ray emission with much better resolution than the natural line width, making HERFD-XAS of particular use for very dilute biological systems. This method has been used to examine the Cu(II) binding site in the amyloid β peptide,[40] to probe metal-containing active sites in nitrogenase[41] and monooxygenase,[42,43] and to examine mercury in brain tissue from the Minamata tragedy.[44] HERFD-XAS overcomes the spectral broadening in conventional XAS, which arises from the short lifetime of the core hole generated by the initial photoexcitation event.[45,46] When the fluorescence is detected with adequately high energy resolution, the observed spectroscopic broadening is no longer dictated by the lifetime of the core hole generated by the primary photoexcitation but is

instead controlled by the lifetime of the core hole generated by the decay of the electron to yield the fluorescent photon and fill the core hole. The resulting spectra are significantly sharper than conventional XAS spectra and provide increased sensitivity for the determination of elemental forms in dilute samples (e.g., <1 ppm Se[47]). It is frequently assumed that HERFD-XAS is identical to XAS with much improved spectroscopic resolution; however, this is not an accurate view of the method. HERFD-XAS is typically recorded as the diagonal of the RIXS plane,[46] and any off-diagonal RIXS intensities may therefore be missing from the recorded HERFD-XAS, although these would be included (but often unresolved) in ordinary XAS.

Comparisons of the X-ray absorption near-edge spectra from conventional XAS and HERFD-XAS of Cu(II)-bound PBT2 in a ratio of excess PBT2/Cu(II) in aqueous surfactant solutions are shown in Figure S.3. The conventional XAS near-edge spectrum of Cu(II) PBT2 shows a small, broad 1s → 3d transition centered at approximately 8979 eV, which is indicative of Cu(II) species and suggests that the photoreduction to Cu(I) is minimal. From HERFD-XAS spectra of Cu(II) PBT2, the 1s → 3d transition is clearly split into two peaks at 8979.0 eV (intensity of 0.023) and 8980.4 eV (intensity of 0.016) (Figure 4A and B; Table 2), which is unlike other Cu(II)-*bis*-8HQs studied previously (Figure 4B; Table 2). Although the EPR spectrum of 1:20 Cu(II)/PBT2 above (Figure 2a and b) is consistent with a single species in solution, the ratios used in XAS analyses (1:2.5 Cu(II)/PBT2) are likely more consistent with the 1:2 Cu(II)/PBT2 EPR spectrum (Figure 2c). In line with this, the split 1s → 3d transition may be an indication of two different coordination environments in solution. Additionally, and in line with our EPR spectra, near-edge fitting of XAS spectra from a titration of Cu(II) into a solution of PBT2 suggests that mixtures of Cu(II) PBT2 complexes form in solution depending on the Cu(II)/PBT2 ratio. For example, fitting of the spectrum of the 2:1 PBT2/Cu solution suggests that it is a best fit to 80% of the 2.5:1 PBT2/Cu spectrum and 20% of the 1:1 PBT2/Cu spectrum, where the ratios indicate the proportion of PBT2 and Cu(II) added to the solution (Figure S.4). While we could not completely rule out the possibility that the split 1s → 3d transition is related to the photoreduction of our initial Cu(II) species, this appears to be unlikely. Comparisons of our Cu(II) PBT2 spectra with chemically reduced Cu(I) standards suggest that there are no peaks in the Cu(I) spectra in the 1s → 3d region (below ~8981 eV).

Previously, many Cu(II)-*bis*-8HQs were shown to have prominent peaks at about 8983 eV, which are attributable to 1s → $4p_z$ + ligand-to-metal charge transfer (LMCT) shake-down transitions, and at ~8987 eV, which were attributed to 1s → $4p_{xy}$ + LMCT shake-down transitions in aqueous solution.[26] This type of transition is often indicative of square-planar Cu(II) coordination geometry;[48–50] however, we have recently shown that halogens in the five- and seven-positions of 8HQ derivatives can impact the intensity of this near-edge transition.[26] The Cu(II)-*bis*-Cl2Q complex was shown to have intensities of 0.14 and 0.84 for the 1s → $4p_z$ and 1s → $4p_{xy}$ + LMCT shake-down transitions, respectively (Table 2; Figure 4A and B).[26] We have previously suggested that substituents in the 2-position can significantly distort the planarity of these complexes such that the planes defined by each 8HQ moiety in Cu(II)-*bis*-MC2Q or Cu(II)-*bis*-AC2Q complexes are separated by ~30°, resulting in a propeller-like structure.[26] These distortions from the expected square-planar structure were also found to systematically decrease the intensity of the 1s → $4p_z$ and 1s →

$4p_{xy}$ + LMCT shake-down transitions, such that their intensities are 0.088 and 0.78 for the MC2Q complex, respectively, and 0.085 and 0.75 for the Cu(II) complex with AC2Q, respectively (Table 2; Figure 4A and B).[26] Aqueous solution spectra of Cu(II) PBT2 complexes show broad shoulders at the energies these transitions typically occur (intensities of ~0.18 and ~0.58 for the 1s → $4p_z$ + LMCT and 1s → $4p_{xy}$ + LMCT transitions, respectively; Table 2; Figure 4A and B), suggesting that the Cu(II) coordination environment is different from that of both the pseudo-square-planar coordination in Cu(II) complexes of Cl2Q and the distorted four-coordinate Cu(II) environments in 2-substituted MC2Q and AC2Q complexes with Cu(II). Additionally, the broadness of the 1s → 4p + LMCT shake-down transitions supports the hypothesis that there is a mixture of different Cu(II)-*bis*-PBT2 complexes in solution. Although we did not observe changes in the near-edge region of our Cu(II) PBT2 spectra, we could not completely rule out the possibility that the shoulder at ~8983.6 eV corresponds to a 1s → 4p transition from a small number of Cu(I) species.

2.3. EXAFS and EXAFS Fourier Transform.

The EXAFS of Cu(II)-bound PBT2 in a ratio of 2.5:1 PBT2/Cu(II) in aqueous surfactant solution is shown in Figure 4C. The EXAFS oscillations of the Cu(II)-PBT2 complex have little high-k structure and lower EXAFS amplitude, $\chi(k) \times k^3$, compared to other pseudo-square-planar Cu(II)-*bis*-8HQ complexes (e.g., CQ).[26] However, the EXAFS oscillations show some similarity to those of distorted four-coordinate Cu(II) complexes observed with other 2-substituted, 5,7-dichlorinated-8HQs, such as MC2Q and AC2Q (Figure 4C). The striking difference is that the EXAFS spectrum of Cu(II) PBT2 has lower intensity than other similar compounds, particularly of the first and second oscillations (Figure 4C). Similar results may be observed from the corresponding EXAFS Fourier transforms (Figure 4D). The primary backscattering peak in the Fourier transform of coplanar Cu(II)-*bis*-Cl2Q is much more intense than that of the PBT2 Cu(II) complex (Figure 4D) and was previously best fit to first shell interactions with 2O (at 1.93 Å) and 2N (at 1.95 Å) ligands.[26] In spectra of many 2-position-substituted 8HQ Cu(II) complexes, the primary backscattering peak has a shoulder or is split into two separate peaks (e.g., MC2Q; Figure 4 D), which is consistent with distinguishably different first shell scattering distances.[26] In best fits of 2-position-substituted 8HQs, the Cu–O was found to be shorter at ~1.90 Å and the Cu–N was longer at ~2.05 Å compared with coplanar 5,7-dihalogenated 8HQs.[26] The primary backscattering peak in the Cu(II) PBT2 Fourier transform similarly shows a peak at ~ 1.9 Å with a shoulder at approximately 2.3 Å (Figure 4 D), which indicates several different distances to the primary backscattering atoms that cannot be fully resolved. Taking the XAS data together, the low-intensity, poorly resolved 1s → 4p + LMCT shake-down transitions in the near-edge, the minimal structure at high k from multiple scattering, and the broad primary backscattering peak in the Fourier transform suggest that (i) the Cu(II) and PBT2 ligands in the Cu(II)-*bis*-PBT2 complex are not all coplanar, (ii) the tertiary amine in the 2-position precludes the formation of a Cu(II)-*bis*-PBT2 complex, and/or (iii) there is significant disorder in the system possibly due to the presence of multiple different Cu(II) PBT2 species and in agreement with EPR spectra.

2.4. Cu(II) Coordination in 2-Substituted 8-Hydroxyquinolines.

Early solution work by Stevenson and Freiser found that 2-position substitution with 2-CH_2NH_2 resulted in a higher Cu(II) complex formation constant (log K_1) for the formation of a Cu(II)-*mono*-8HQ complex compared with 8HQ and 2-methyl-8HQ and suggested that this was due to tridentate Cu(II) coordination (Table 3).[51] However, the 2-CH_2NH_2 substituted 8HQ had a lower log K_2 value for the formation of a Cu(II)-*bis*-8HQ complex compared with that of 8HQ and 2-methyl-8HQ (Table 3), and the authors proposed that one of the ligands, most likely the 2-CH_2NH_2 ligand, must be displaced in order to form the Cu(II)-*bis*-8HQ complex.[51] These authors also mention the possibility that the phenolate oxygen might be released from the coordination sphere such that the Cu(II) remains bound to the pyridine nitrogen and the 2-position amine nitrogen in the Cu(II)-*bis*-8HQ complex.[51] Lower log K values were reported for the formation of Cu(II) complexes with 2-CHNOH and 2-CH_2OH substitution of 8HQ, compared with 2-H and 2-CH_3 (Table 3),[51] suggesting that these substituents did not coordinate and instead sterically hindered Cu(II)-*bis*-8HQ complex formation to a greater extent than 2-CH_3.[51] Stevenson and Freiser proposed that electron-withdrawing 2-position substituents would result in bidentate 8HQ ligands; however, small, electron-donating 2-position substituents would result in tridentate 8HQ ligands.[51]

Recent analyses by Sgarlata et al. suggest a stability constant of log K_1 = 13.61 for the formation of a Cu(II)-*mono*-PBT2 complex and a log K_2 value of 5.95 for the formation of a Cu(II)-*bis*-PBT2 complex (Table 3).[32] It is possible, as Sgarlata et al. suggested, that the low log K_2 value for the formation of Cu(II)-*bis*-PBT2 means that this complex is destabilized because of steric hindrance and is unlikely to form in solution.[32] However, the low log K_2 value may also be due to the release of either the 2-position amine nitrogen or the phenolate oxygen from the tridentate Cu(II)-*mono*-PBT2 chelate complex in order to form the bidentate Cu(II)-*bis*-PBT2 chelate complex, as initially proposed by Stevenson and Freiser for other 2-methyl-8HQ derivatives.[51]

Stevenson and Freiser also note that metal complexes with tridentate 8HQ ligands might preferentially form in solid samples compared with solutions.[51] In line with this proposal is a recent study by Nguyen et al.[29] that suggested the solution structures of Cu(II)-PBT2 differ considerably from those indicated by the crystal structure. This study used the results of X-ray crystallography, EPR, NMR, and UV–visible absorption spectroscopy to propose four structures for Cu(II)-PBT2, including a five-coordinate Cu(II)-*bis*-PBT2 crystal structure with coordination from the tertiary amine in the 2-position (i.e., CSDS entry WAXPIX), and three calculated Cu(II)-*mono*-PBT2 structures with H_2O and Cl^- ligands.[29]

Other than the crystal structure of Cu(II)-*bis*-PBT2 (i.e., CSDS entry WAXPIX), there is only one crystallographic example of tridentate coordination of Cu(II) by 8HQs with a 2-position amine group of formula 2-CH_xNR_x in the Cambridge Structural Database (i.e., CSDS entry FEXYAL[55]), and no bidentate examples could be found. This crystal structure, FEXYAL, shows Cu(II)-*bis*-8HQ coordination in an octahedral-type coordination environment,[55] with both 8HQs acting as tridentate ligands. Few crystal structures suggest the formation of Cu(II)-*mono*-8HQ complexes and those that do often portray tetradentate coordination with two ligands from the 2-position substituent (e.g., CSDS IMUFAY,[56]

FEXXOY,[55] and FEXXUE[55]), which is not possible for PBT2. Similarly, one crystal structure shows tetradentate coordination of one 8HQ, including the coordination of two ligands from the 2-position substituent and bidentate coordination of the second 8HQ in a *bis* complex (i.e., CSDS FEXXIS[55]). Additionally, one crystal structure shows a dimeric species in which two Cu(II) moieties are each coordinated by a tridentate 8HQ with a fourth ligand from the phenolate oxygen of another tridentate 8HQ Cu(II) complex (i.e., CSDS ACUZUT[57]). However, similar complex structures for the Cu(II)-*bis*-PBT2 complex can likely be ruled out because a Cu(II)···Cu(II) interaction would be expected at ~3 Å, and this is not observed in our EXAFS spectra or EXAFS Fourier transforms. Collectively, these structures provide support for Cu(II) coordination by 8HQs with 2-position amines of formula 2-CH_xNR_x and suggest that the strain imposed by two adjacent five-membered chelate rings is not sufficient to prevent the crystallographic formation of tridentate 8HQ Cu(II) complexes. However, as has been proposed previously, the solution structure may differ from that found in crystals.

2.5. Density Functional Theory Calculations.

Density functional theory (DFT) geometry-optimized potential structures of Cu(II)-*bis*-PBT2 complexes are shown in Figure 5. The Cu(II)-*bis*-PBT2 structures proposed in the literature are compared with other possible Cu(II) coordination geometries and are listed in order of decreasing energy. Stevenson and Freiser had previously proposed that in binding a second 8HQ moiety it was possible that either the 2-position amine or the 8-position phenolate oxygen might be released from the coordination sphere.[51] We then extrapolated that there was potential for the formation of both a 4N and a 3 N 1 O coordination environment. The resulting potential 4N Cu(II)-*bis*-PBT2 complex, formed by Cu(II) coordination through the two pyridine nitrogens and the two 2-position amine nitrogens, was approximately 300 kJ/mol higher than the lowest-energy structure, which was found to be a 3 N 1 O coordination environment (Figure 5). Our 3 N 1 O coordination environment—a Cu(II) coordination environment that has not been described previously for 2-position-substituted 8HQs with 2-CH_2NR_x substituents—was formed through coordination of the pyridine nitrogen and the 2-position amine nitrogen of one PBT2 and the pyridine nitrogen and the phenolate oxygen of another PBT2. This coordination environment may occur in a pseudo-*trans* or pseudo-*cis* conformation according to the orientation of the phenolate oxygens and pyridine nitrogens of the 8HQ moiety; however, there is almost no energetic difference between the two conformations (<0.2 kJ/mol). A distorted *trans* 2 N 2 O coordination environment formed by the two pyridine nitrogens and the two phenolate oxygens was found to be approximately 20 kJ/mol higher than that for the 3 N 1 O complexes (Figure 5). Similar to other 2-position-substituted 8HQs, the typical 2 N 2 O coordinate complex of Cu(II)-*bis*-PBT2 is distorted from the pseudo-square-planar coordination environments found in coplanar Cu(II)-*bis*-8HQ complexes with 8HQs that lack 2-position substituents such that one of the 8HQ moieties is rotated approximately 30° from the plane defined by the other 8HQ moiety (Table 2; Table S.2). The $\tau 4$ and $\tau 4'$ parameter values,[58,59] where 0 is representative of square-planar geometry and 1 is representative of tetrahedral geometry, calculated for the 2 N 2 O complex are 0.39 and 0.37, respectively (Table S.2). These values suggest that this symmetric four-coordinate complex is significantly distorted from coplanarity, similar to 2-position-substituted 8HQs

investigated previously.[26] The 3 N 1 O complex is further distorted such that the Cu(II) coordination environment approaches tetrahedral geometry with $\tau 4$ and $\tau 4'$ parameter values of 0.97 and 0.68, respectively (Table S.2).

Although 3 N 1 O coordination environments for the Cu(II)-*bis*-PBT2 complex are the lowest-energy structures, the energy barrier ($\Delta E^{\ddagger}$) for converting between 3 N 1 O and 2 N 2 O coordination environments was calculated to be 439.1 kJ/mol for the pseudo-*trans* conformation and 410.0 kJ/mol for the pseudo-*cis* conformation. To account for the charge difference between $[3\text{ N }1\text{ O}]^+$ complexes with a protonated 8-position OH group and the neutral 2 N 2 O complex in transition-state calculations, an additional proton was placed on the 2-position amine in the initial 2 N 2 O reactant structure such that the 2-position substituent was $2\text{-}CH_2NH(CH_3)_2$ and resulted in a $[2\text{ N }2\text{ O}]^+$ complex. On the basis of these results, it is unlikely that the 3 N 1 O and 2 N 2 O coordination environments would interconvert in solution, and it is highly probable that mixtures of these species might coexist in solution. However, calculated energy barriers to interconversion are often underestimated and unreliable.[60]

2.6. Curve Fitting of the EXAFS.

Scattering paths for geometry-optimized structures of Cu(II)-bound PBT2 complexes were calculated using FEFF825 and fit to the EXAFS data in the curve-fitting program, OPT, in EXAFSPAK.[61] As we have described previously, the orientation of the Cu(II) center, the phenolate oxygen, and the 7-position halogen in halogenated 8HQ derivatives at close to 180° allows for the unusual opportunity to use EXAFS to probe the geometry of Cu(II)-*bis*-8HQ complexes. It is unusual to detect backscattering atoms ≳5 Å from the absorbing atom (i.e., Cu) in solution complexes. In 5,7-halogenated-8HQs, the distant halogen substituents are detected (i) because the halogen substituents are high-Z atoms, giving rise to a large backscattering amplitude (ii) because the halogens are connected to the Cu(II) via a relatively rigid ring system, minimizing the possible disorder in the Cu···X distances, and (iii) because multiple scattering involving the intervening oxygen or carbon atom in the planar 8HQ moiety enhances the EXAFS amplitude when paths approach colinearity (i.e., approach 180°; Figure S.5; Table S.2). With this in mind and with spectral comparisons to other Cu(II) complexes with 5,7-dichlorinated-8HQ derivatives, it appears that the Cu(II)–O···Cl path to the 7-position Cl substituent in the Cu(II)-*bis*-PBT2 more closely approaches an optimal, linear backscattering angle than the parent Cu(II)-*bis*-Cl2Q complex (Figure 4C; Table S.2). Similar to Cu(II)-*bis*-MC2Q and Cu(II)-*bis*-AC2Q, Cu(II)-*bis*-PBT2 has some higher-frequency EXAFS oscillations at higher k compared with Cu(II)-*bis*-Cl2Q (Figure 4C). These high-frequency EXAFS oscillations are likely enhanced through multiple scattering to the distant 5- and 7-position chlorine substituents.

Possible structures for Cu(II)-PBT2 were fit to the Cu(II) K-edge EXAFS; the best curve-fitting results for 1:2.5 Cu(II)/PBT2 are shown in Figure 6A and detailed in Table S.4. Alternative fits comparing the coplanar, pseudo-square-planar structure typical of 2-H 8HQs, the square pyramidal structure proposed by Kenche et al.,[27] and the Cu(II)-*bis*-PBT2 crystal structure[29] are shown in Figure S.6 and described in Table S.3. The EXAFS of Cu(II)-bound PBT2 formed with excess PBT2 is best fit to a distorted 2 N 2 O coordination environment

(Figure 6A), similar to distorted *trans* coordination environments previously described for 2-position-substituted 8HQs.[26] Although distorted 3 N 1 O coordination environments where the phenolate oxygen and pyridine nitrogen are arranged *cis* or *trans* were found to be lower energy by DFT, these coordination environments were found to comprise a small proportion of the species in solution (Figure 6A). Because the 3 N 1 O coordination environment appears to be less abundant in solution and because of the noise in the EXAFS at higher *k*, the inclusion of scattering paths for a 3 N 1 O coordination environment did not improve the fit. Additionally, the possibility of both *cis* and *trans* arrangements for the 3 N 1 O complex increases the number of potential coordination environments and makes the EXAFS fitting very challenging.

Steric effects likely preclude the formation of either a five- or six-coordinate Cu(II)-*bis*-PBT2 complex in which one or both PBT2 compounds, respectively, would act as tridentate ligands. Attempts to find an energy minimum for 5- or 6-coordinate Cu(II)-*bis*-PBT2 complexes always resulted in the tertiary amine N being pushed approximately 3–4 Å from the Cu(II) center. In the best-fit 2 N 2 O structure, the Cu(II)–O···Cl path is slightly closer to linearity at 176.5° compared with 174.4° previously found for the best-fit coplanar structure of Cu(II)-*bis*-Cl2Q and is similar to those found for other distorted Cu(II)-*bis*-8HQ complexes (Table S.2).[26]

Although the spectra of 1:1 PBT2/Cu(II) are likely a mixture of at least three species, including the Cu(II)-*bis*-PBT2 complex and aqueous Cu(II), we attempted to fit the average Cu(II) coordination environment. The best fit was found to be to a tridentate PBT2 ligand with an additional coordinating Cl^- ligand (Figure 6B), suggesting that this may be the major species in the mixture. However, this fit describes the average species in the mixture and may not accurately describe the individual components. Further studies using techniques that can distinguish the different proposed species are required to better describe this mixture. Our fitting results, as well as the findings from previous studies,[29,32,51] may suggest that PBT2 initially binds Cu(II) as a tridentate ligand. Under conditions of excess PBT2, formation of the Cu(II)-*bis*-PBT2 complex results in the release of one of the initial three ligands, likely the tertiary amine, although the release of the phenol oxygen is also possible.

The concentration of copper in the human brain has been previously found to be 3.32 ± 1.50 μg/g,[62] with copper concentrations in amyloid plaques reported to be as high as 25.0 ± 7.8 μg/g in AD patients.[63] [The study by Lovell et al.[63] used formalin fixed brain tissue, which is known to result in metal contamination in some cases (e.g., copper) and elemental depletion in other cases (e.g., potassium).[64,65] Therefore, the reported copper concentrations may be somewhat overestimated.[65]] PBT2 concentrations were reported to be 318.1 ± 75.1 ng/g in the brain of Alzheimer's model mice 2 h after an oral dose of 30 mg/kg.[2] This would seem to suggest that there is likely to be at least 10 times more copper in the AD brain than PBT2. However, much of this copper is likely to be intracellular, bound strongly to various copper proteins and chaperones, and in the monovalent form. PBT2 is likely to chelate only weakly bound Cu(II), with the goal being to chelate weakly bound, redox-active, toxic Cu(II) from extracellular amyloid plaques. PBT2 is likely to initially bind Cu(II) in a tridentate Cu(II)-*mono*-PBT2 complex, and although it is difficult to predict given the

information currently available, Cu(II)-*bis*-PBT2 complexes may form *in vivo* depending on the local environment (e.g., the relative concentrations of available Cu(II), PBT2, and copper-binding proteins and small molecules).

3. CONCLUSIONS

3.1. Structures of PBT2 Complexes of Cu(II).

It has been proposed that in the formation of Cu(II) 8HQ complexes, where 8HQ has a 2-position substituent of formula 2-CH_2NR_x, the 2-position amine may be involved in Cu(II) coordination.[51] Furthermore, it has been proposed that a tridentate Cu(II)-*mono*-8HQ complex may form first and that one of the three 8HQ ligands—either the 2-position amine or the phenolate oxygen—must be released in the formation of a Cu(II)-*bis*-8HQ complex. On the basis of these hypotheses, we propose several potential solution structures for the Cu(II)-*bis*-PBT2 complex. Although the 2-position ligand is most likely to be displaced such that Cu(II) is bound through the phenolate oxygen and the pyridine nitrogen, the phenolate oxygen may instead be displaced such that Cu(II) remains bound to the 2-position amine and the pyridine nitrogen (Figure 8). The second PBT2 moiety might then coordinate as a bidentate chelate through either the 8-position phenolate oxygen or the 2-position amine as well as the pyridine nitrogen. The 4 N complex in which Cu(II) is coordinated by two pyridine nitrogens and two amine nitrogens was found to be energetically unfavorable. However, 3 N 1 O complexes in which the Cu(II) is coordinated by the pyridine nitrogen and the 2-position amine in one bidentate PBT2 and by the pyridine nitrogen and phenolate oxygen in the other bidentate PBT2 in either a *cis* or *trans* conformation were found to be the most energetically favorable Cu(II)-*bis*-PBT2 structures (Figure 8). A distorted structure similar to that found previously for 2-position-substituted 8HQs, in which the Cu(II) is coordinated by two bidentate PBT2 chelates though the phenolate oxygens and pyridine nitrogens in a *trans* conformation, was found to be only slightly less energetically favorable than the 3 N 1 O conformations. Because the energy barrier is sufficient to prevent interconversion between these complexes, it is likely that a mixture of these coordination environments coexists in solution. The mixture is likely to be influenced by solution conditions such as the pH and relative concentrations of PBT2 and Cu(II), which might explain the different results obtained in different studies.

3.2. Implications for Future Drug Design.

We have shown previously that the halogen substituents in 5,7-halogenated-8-hydroxyquinolines can impact the hydrophobicity of both the compound and its resultant Cu(II) complex.[26] Additionally, we have shown previously that substitution in the 2-position of 8HQs can alter the Cu(II) coordination environment, with even 2-CH_3 resulting in significant distortions to the coplanar 4-coordinate *bis* complex formed with 2-H 8HQs.[26] We find herein with PBT2 that 2-position substitution with a 2-$CH_2N(CH_3)_2$ group results in the potential formation of a completely different Cu(II) coordination environment in the *bis* complex. The superior anti-AD effects of PBT2 treatment, specifically its increased ionophoric activity compared with CQ,[2] may be linked to its potential to act as a tridentate chelate for Cu(II), in addition to its other properties such as greater blood–brain barrier permeation than other 8HQs.[2] Additionally, the flexibility for tridentate or bidentate chelate

formation, with several possible Cu(II) binding ligands (i.e., the phenyl oxygen, the pyridine nitrogen, and the tertiary amine nitrogen), may make PBT2 an effective drug for Cu(II) sequestration and prevent aberrant redox reactions, such as Fenton-type chemistry, related to loosely bound, toxic Cu(II) in the Alzheimer's disease brain.

4. MATERIALS AND METHODS

4.1. Synthesis of PBT2.

5,7-Dichloro-2-[(dimethylamino)-methyl]-8-hydroxyquinoline (PBT2) was prepared as a hydrochloric salt as previously described.[64] Briefly, triethylamine (0.55 mL) was added dropwise to a stirred solution of 5,7-dichloro-8-hydroxyquinoline-2-carboxaldehyde (1.0 g, 4.13 mmol) and dimethylamine hydrochloride (365 mg, 4.48 mmol) in 1,2-dichloroethane (50 mL) over 5 min. Sodium triacetoxyborohydride (1.2 g, 5.66 mmol) was then added portionwise over 5 min, and the mixture was stirred at room temperature overnight. Dichloromethane (100 mL) was added, the mixture was washed with saturated sodium bicarbonate (50 mL × 3), dried using Na_2SO_4, and concentrated. The resultant residue was extracted with diethyl ether (50 mL × 4), and the ethereal extracts were combined and concentrated. HCl (5 mL) was added, and the mixture was concentrated *in vacuo* twice. After washing with dichloromethane, PBT2·HCl was obtained as a pale straw-colored solid (yield ≈ 15–30%).

4.2. XAS Sample Preparation.

A stock solution of dodecyl trimethylammonium bromide (DTAB) was prepared to a final concentration of 400 mM in 100 mM 3-(*N*-morpholino)propane-sulfonic acid (MOPS) at pH 7.4. Solutions were heated to ~60 °C and sonicated for ~10 min or until completely dissolved. Aqueous Cu(II) PBT2 samples were prepared by diluting PBT2 from a 10 mM stock to a final concentration of 5 mM (excess PBT2/Cu sample) or 2 mM (1:1 PBT2/Cu sample). Cu(II), from an aqueous stock solution of 100 mM $CuCl_2$, was then added to the surfactant solution to a final concentration of 2 mM. Aqueous samples were loaded into 3 mm acrylic sample cuvettes sealed with metal-free tape, flash frozen in a slurry of isopentane cooled in liquid nitrogen, and stored at 77 K prior to experimentation.

4.3. Synchrotron High-Energy-Resolution Fluorescence-Detected X-ray Absorption Spectroscopy.

Near-edge HERFD-XAS measurements were carried out on BL 6–2 at the Stanford Synchrotron Radiation Lightsource (SSRL) with the SPEAR3 storage ring containing 500 mA at 3.0 GeV. Using a setup similar to that previously described for our Se HERFD-XAS,[65] a Si(311) double-crystal monochromator with an energy resolution at the Cu K-edge of ~0.3 eV was used with a six-element Johann-type array of Si(444) crystal analyzers to record the Cu Kα_1 emission.[66] Harmonic rejection was achieved by setting the cutoff energy of the upstream Rh-coated mirror to 18 keV. Incident and transmitted X-rays were monitored using helium-filled and nitrogen-filled gas ionization chambers, respectively. HERFD-XAS spectra were recorded by monitoring a fixed emission energy located at the centroid of the Cu Kα_1 emission peak obtained with a nonresonant incident X-ray energy of 9300 eV. This emission energy was determined on a sample-by-sample basis by recording an emission scan

prior to HEFRD-XAS data acquisition and determining its centroid. The variation in emission energies from sample to sample was found to be small for the species examined here, within about 0.1 eV. The HERFD-XAS spectrum was then recorded by scanning the incident X-ray energy, essentially interrogating the diagonal of the resonant inelastic X-ray scattering (RIXS) plane. An in-hutch photon shutter was used to prevent exposure of the sample when data were not actively being recorded. Aluminum filters upstream of the incident ion chamber were used to minimize X-ray exposure and the resulting photodamage. Samples were maintained at 10 K using a liquid helium flow cryostat (Oxford Instruments, Abingdon, U.K.) and were inclined at 45° with respect to the incident X-ray beam to facilitate the measurement of X-ray fluorescence, giving an effective incident X-ray path length of 2.8 mm. Energy calibration of the monochromator was determined relative to the lowest-energy inflection of a copper foil, which was assumed to be 8980.3 eV. HERFD-XAS data sets are an average of 20 individual sweeps; each sweep was collected at different sample positions such that the beam interrogated a fresh spot on the sample to minimize photodamage. The time taken for the scan to traverse the structured region of the data was approximately 30 s. Spectra of successive scans were compared for loss of the 1s → 3d transition, which is often indicative of photoreduction.[67] Data reduction and analyses were carried out as previously described[68] using the EXAFSPAK suite of computer programs.[61]

4.4. Synchrotron X-ray Absorption Spectroscopy.

Cu K-edge XAS measurements were conducted at SSRL using the data acquisition program XAS-Collect.[69] Cu K-edge data were collected on biological XAS beamline (BL) 7–3 with the SPEAR storage ring containing 500 mA at 3.0 GeV. Beamline 7–3 utilizes a Si(220) double-crystal monochromator and a rhodium-coated vertically collimating mirror upstream of the monochromator, which achieves harmonic rejection by adjusting the mirror cutoff angle (i.e., 12 keV for Cu). Samples were maintained at ~10 K using a liquid helium flow cryostat during data collection. Incident and transmitted X-rays were measured using nitrogen-filled gas ionization chambers. Fluorescence spectra were collected by monitoring the Kα fluorescence using a 30-element germanium detector. The monochromator energy was calibrated to the first peak of the first derivative of the Cu K-edge (8980.3 eV) through reference to a standard Cu foil measured simultaneously with the sample. Each data set is a collection of a minimum of six scans. To decrease the risk of photoreduction of Cu(II) compounds, samples were scanned at multiple positions on the same sample (i.e., using a 0.5 × 12 mm^2 beam and 0.5 mm vertical movements), and the near edges of successive scans were compared for the loss of the 1s → 3d transition, which is often indicative of photoreduction.

4.5. Density Functional Theory Calculations.

DFT calculations utilized $Dmol^3$ Materials Studio 7.0, specifically, $Dmol^3$ geometry optimization employing the generalized gradient approximation (GGA)[70] and Perdew-Burke-Ernzerhof (PBE)[71] functionals as well as meta-GGA (m-GGA)[72] and M11-L.[73] Optimization calculations used all-electron core treatment and were calculated *in vacuo* (i.e., without a solvent reaction field). Calculations used symmetry parameters where appropriate to define the point group of Cu(II) 8HQ complexes. To compare the energy of different Cu(II) coordination environments in Cu(II)-*bis*-PBT2 with the protonated $[3\ N\ 1\ O]^+$ and

doubly protonated [4 N]$^{2+}$ complex, the charge difference was accounted for using the energy of small, neutral, and charged compounds. Specifically, twice the energy calculated for $[NH(CH_3)_3]^+$ was added to that of the neutral species, and twice the energy calculated for $N(CH_3)_3$ was added to that of the 2+ charged species. The energy calculated for $[NH(CH_3)_3]^+$ and $N(CH_3)_3$ was added to 1+ species.

Transition-state calculations to determine energy barriers used m-GGA and M11-L functionals. To account for the charge difference between [3 N 1 O]$^+$ complexes with a protonated 8-position OH group and the neutral 2 N 2 O complex, an additional proton was placed on the 2-position amine in the initial 2 N 2 O reactant structure such that the 2-position substituent was 2-$CH_2NH(CH_3)_2$ and resulted in a [2 N 2 O]$^+$ complex.

4.6. EPR Sample Preparation.

Samples for EPR spectroscopy were prepared as described above for XAS sample preparation (Section 4.2). $^{63}CuCl_2$ was prepared by dissolving ^{63}CuO (>99% ^{63}Cu, Isoflex USA, San Francisco, CA) in concentrated HCl and evaporating to dryness. An aqueous stock solution of 20 mM $^{63}CuCl_2$ was then prepared by dissolving the $^{63}CuCl_2$ powder in deionized water. Aqueous ^{63}Cu(II) PBT2 samples were prepared by dissolving PBT2 to a final concentration of 0.25, 0.5, or 5 mM (for ^{63}Cu(II)/ PBT2 ratios of 1:1, 1:2, and 1:20, respectively). Aqueous ^{63}Cu(II) was then added to the surfactant solution to a final concentration of 0.25 mM. Pure isotope ^{63}Cu was used to avoid inhomogeneous broadening of the EPR lines that would otherwise be present with a mixture of naturally occurring ^{63}Cu and ^{65}Cu isotopes. Aqueous samples were loaded into 5-mm-external-diameter quartz tubes and frozen using liquid nitrogen.

4.7. Electron Paramagnetic Resonance.

X-band EPR (~9.43 GHz) used a Bruker EMX spectrometer with a Bruker ER 4122SHQE resonator. Typical spectrometer conditions were 0.1 mT modulation amplitude, 5 mW applied microwave power, and 121 K temperature. The spectrum was an average of eight 83.89 s sweeps, with 2048 points per scan. EPR powder line shape simulation used a modified version of the QPOW program.[74,75] The difference spectrum in Figure 2e was generated by the subtraction of spectrum b (excess PBT2/Cu) from spectrum d (1:1 PBT2/Cu). Spectra were normalized by amplitude, aligned, and then subtracted in 0.1 increments until a point was reached in which additional subtraction resulted in negative (inverted) spectral features in the region below 320 mT. The amplitude of the generated difference spectrum was determined to be 0.56; therefore, the proportion of the excess PBT2 Cu(II) complex subtracted was 0.44 or ~44%. We estimate that this is accurate to approximately ±5%.

4.8. EXAFS Curve-Fitting.

The *ab initio* theoretical phase and amplitude of energy-minimized molecular models were calculated using FEFF825.[76,77] The calculated scattering paths were then fit to the EXAFS using curve-fitting program OPT (a component of EXAFSPAK). The number (N) of each type of backscattering atom was not refined individually but was instead fit as an integer based on the molecular model. Refinable parameters included the following: distance (R)

between Cu and the backscattering atom, mean square deviation in R (Debye-Waller factor, σ^2), and the energy offset (ΔE_0) to the nominal threshold energy (9000 eV). R parameters were fit as a group of linked paths; R values listed in Tables S.3 and S.4 with a standard error in parentheses were allowed to float within the refinement. The σ^2 values for each distance, R, were refined as a group for the entire energy-minimized structural model. The fit error function F is defined as

$$F = \left\{ \frac{\sum k^6 \left(\chi_{\text{calc}} - \chi_{\text{expt}}\right)^2}{\sum \chi_{\text{expt}}{}^2} \right\}^{1/2} \quad (1)$$

Noise contributions with frequencies higher than the longest bond length in the EXAFS fit were estimated, as previously described,[78] by computing the product of the Cu–N phase-corrected discrete Fourier transform. The discrete Fourier transform contains all frequencies supported by the k-space data, extending to

$$R_{\text{max}} = \frac{2\pi}{\delta k} \quad (2)$$

where δk is the minimum k-space point separation. The back-transform of this was then computed and used to estimate F', employing eq 1. Fitting parameters for each best-fit model are summarized in Tables S.3 and S.4.

Supplementary Material

Refer to Web version on PubMed Central for supplementary material.

ACKNOWLEDGMENTS

Research carried out at the University of Saskatchewan was supported by the Natural Sciences and Engineering Research Council of Canada (NSERC), the Canadian Institutes of Health Research (CIHR), and the Saskatchewan Health Research Foundation (SHRF). I.J.P and G.N.G are Canada Research Chairs. K.L.S held an Alexander Graham Bell Canadian Graduate Scholarship from NSERC and gratefully acknowledges travel support from a Michael Smith Foreign Study Supplement. H.H.H. acknowledges financial support from the Australian Research Council (DP140100176). Research reported in this publication was supported by the National Institutes of Health through a grant to G.L.M (GM065790). Cu K-edge X-ray absorption spectroscopy (XAS) was carried out at the Stanford Synchrotron Radiation Lightsource (SSRL). Use of the Stanford Synchrotron Radiation Lightsource, a SLAC National Accelerator Laboratory, is supported by the U.S. Department of Energy, Office of Science, Office of Basic Energy Sciences under contract no. DE-AC02-76SF00515. The SSRL Structural Molecular Biology Program is supported by the DOE Office of Biological and Environmental Research and by the National Institutes of Health, National Center for Research Resources, Biomedical Technology Program (P41RR001209).

ABBREVIATIONS

AC2Q	5,7-dichloro-8-hydroxyquinoline-2-carboxaldehyde
8HQ	8-hydroxyquinoline
Aβ	amyloid beta
AD	Alzheimer's disease
CQ	clioquinol, 5-chloro-7-iodo-8-hydroxyquinoline

Cl2Q	5,7-dichloro-8-hydroxyquinoline
DTAB	dodecyl trimethylammonium bromide
EPR	electron paramagnetic resonance spectroscopy
EXAFS	extended X-ray absorption fine structure
FT	Fourier transform
HD	Huntington's disease
HERFD-XAS	high-energy-resolution fluorescence-detected X-ray absorption spectroscopy
MC2Q	5,7-dichloro-8-hydroxy-2-methylquinoline
MOPS	3-(N-morpholino)propanesulfonic acid
NMR	nuclear magnetic resonance spectroscopy
PBT2	5,7-dichloro-2-[(dimethylamino)methyl]-8-hydroxyquinoline
XAS	X-ray absorption spectroscopy

REFERENCES

(1). Cherny R; Atwood CG; Xilinas M; Gray DN; Jones WD; McLean CA; Barnham KJ; Volitakis I; Fraser FW; Kim Y; Huang X; Goldstein LE; Moir RD; Lim JT; Beyreuther K; Zheng H; Tanzi RE; Masters CL; Bush AI Treatment with a copper-zinc chelator markedly and rapidly inhibits -amyloid accumulation in Alzheimer's disease transgenic mice. Neuron 2001, 30 (3), 665–676. [PubMed: 11430801]

(2). Adlard PA; Cherny RA; Finkelstein DI; Gautier E; Robb E; Cortes M; Volitakis I; Liu X; Smith JP; Perez K; Laughton K; Li Q-X; Charman SA; Nicolazzo JA; Wilkins S; Deleva K; Lynch T; Kok G; Ritchie CW; Tanzi RE; Cappai R; Masters CL; Barnham KJ; Bush AI Rapid restoration of cognition in Alzheimer's transgenic mice with 8-hydroxyquinoline analogs is associated with decreased interstitial Aβ. Neuron 2008, 59 (1), 43–55. [PubMed: 18614028]

(3). Ritchie CW; Bush AI; Mackinnon A; Macfarlane S; Mastwyk M; MacGregor L; Kiers L; Cherny R; Li QX; Tammer A; Carrington D; Mavros C; Volitakis I; Xilinas M; Ames D; Davis S; Volitakis I; Xilinas M; Ames D; Davis S; Beyreuther K; Tanzi RE; Masters CL Metal-protein attenuation with iodochlorhydroxyquin (clioquinol) targeting A amyloid deposition and toxicity in Alzheimer disease - A pilot phase 2 clinical trial. Arch. Neurol 2003, 60 (12), 1685–1691. [PubMed: 14676042]

(4). Ibach B; Haen E; Marienhagen J; Hajak G Clioquinol treatment in familiar early onset Alzheimer's disease: A case report. Pharmacopsychiatry 2005, 38 (4), 178–179. [PubMed: 16025421]

(5). Lannfelt L; Blennow K; Zetterberg H; Batsman S; Ames D; Hrrison J; Masters CL; Targum S; Bush AI; Murdoch R; Wilson J; Ritchie CW Safety, efficacy, and biomarker findings of PBT2 in targeting A as a modifying therapy for Alzheimer's disease: A phase IIa, double-blind, randomised, placebo-controlled trial. Lancet Neurol. 2008, 7 (9), 779–786. [PubMed: 18672400]

(6). Faux NG; Ritchie CW; Gunn A; Rembach A; Tsatsanis A; Bedo J; Harrison J; Lannfelt L; Blennow K; Zetterberg H; Ingelsson M; Masters CL; Tanzi RE; Cummings JL; Herd CM; Bush AI PBT2 rapidly improves cognition in Alzheimer's disease: Additional phase II analyses. J. Alzheimer's Dis 2010, 20 (2), 509–516. [PubMed: 20164561]

(7). Konagaya M; Matsumoto A; Takase S; Mizutani T; Sobue G; Konishi T; Hayabara T; Iwashita H; Jujihira T; Miyata K; Matsuoka Y Clinical analysis of longstanding subacute myelo-opticoneuropahty: Sequelae of clioquinol at 32 years after its ban. J. Neurol. Sci 2004, 218, 85–90. [PubMed: 14759638]

(8). Shaumburg HH Clioquinol. In Experimental and Clinical Neurotoxicology, 2nd ed.; Spencer PS, Schaumburg HH, Ludolph AC, Eds.; Oxford University Press: Oxford, 2000; pp 397–400.

(9). Kaeser HE Transient global amnesia due to clioquinol. Acta Neurol. Scand 1984, 70 (100), 175–179.

(10). Schaumburg H; Herskovitz S Copper deficiency myeloneuropathy: A clue to clioquinol-induced subacute myelo-optic neuropathy? Neurology 2008, 71 (9), 622–623. [PubMed: 18725588]

(11). Tamura Z; Yoshioka M; Imanari T; Fukaya J; Kusaka J; Samejima K Identification of green pigment and analysis of clioquinol in specimens from patients with subacute myelo-optic-neuropathy. Clin. Chim. Acta 1973, 47, 13–20. [PubMed: 4270607]

(12). Tjälve H The aetiology of SMON may involve an interation between clioquinol and environmental metals. Med. Hypotheses 1984, 15, 293–299. [PubMed: 6240588]

(13). Arbiser JL; Kraeft S-K; van Leeuwen R; Hurwitz SJ; Selig M; Dickersin GR; Flint A; Byers HR; Chen LB Clioquinol-zinc chelate: A candidate causative agent of subacute myelo-optic neuropathy. Mol. Med 1998, 4 (10), 665–670. [PubMed: 9848083]

(14). Kumar N; Gross JB; Ahlskog JE Copper deficiency myelopathy produces a clinical picture like subacute combined degeneration. Neurology 2004, 63 (1), 33–39. [PubMed: 15249607]

(15). Barnham KJ; Bush AI Biological metals and metal-targeting compounds in major neurodegenerative diseases. Chem. Soc. Rev 2014, 43, 6727–6749. [PubMed: 25099276]

(16). Prana Biotechnology Limited. Prana Biotechnology announces preliminary results of Phase 2 IMAGINE trial of PBT2 in Alzheimer's disease; CISION PR Newswire: Melbourne, Australia, 2014. Accessed 14/09/2020 from https://www.prnewswire.com/news-releases/prana-biotechnology-announces-preliminary-results-of-phase-2-imagine-trial-of-pbt2-in-alzheimers-disease-253173581.html.

(17). Prana Biotechnology Limited. Prana Announces that PBT2 Reduces Cognitive Impairment Caused by Tau Protein Accumulation; Prana Biotechnology: Melbourne, Australia, 2013; Vol. 2018. Accessed 14/09/2020 from https://alteritytherapeutics.com/investor-centre/news/2013/07/17/prana-announces-that-pbt2-reduces-cognitive-impairment-caused-by-tau-protein-accumulation/.

(18). Prana Biotechnology Limited, Prana Announces Successful Phase 2 Results in Huntington Disease Trial 2014. Accessed 14/09/2020 from https://alteritytherapeutics.com/investor-centre/news/2014/02/18/prana-announces-successful-phase-2-results-huntington-disease-trial/.

(19). Huntington Study Group Reach2HD Investigators, Safety, Tolerability, And Efficacy of PBT2 in Huntington's Disease: A Phase 2, Randomised, Double-Blind, Placebo-Controlled Trial. Lancet Neurol. 2015, 14 (1), 39–47. [PubMed: 25467848]

(20). Nguyen T; Hamby A; Massa SM Clioquinol down-regulates mutant huntingtin expression *in vitro* and mitigates pathology in a Huntington's disease mouse model. Proc. Natl. Acad. Sci. U. S. A 2005, 102 (33), 11840–11845. [PubMed: 16087879]

(21). Cherny R; Ayton S; Finkelstein DI; Bush AI; McColl G; Massa SM PBT2 reduces toxicity in a C. elegans model of polyQ aggregation and extends lifespan, reduces striatal atrophy and inproves motor performance in the R6/2 mouse model of Huntington's disease. J. Huntington's Dis 2012, 1, 211–219. [PubMed: 25063332]

(22). Dorsey R Effect of PBT2 in patients with early to mid stage Huntington disease (Reach2HD). https://clinicaltrials.gov/ct2/show/study/NCT01590888.

(23). Crouch PJ; Savva MS; Hung LW; Donnelly PS; Mot AI; Parker SJ; Greenough MA; Volitakis I; Adlard PA; Cherny R; Masters CL; Bush AI; Barnham KJ; White AR The Alzheimer's therapeutic PBT2 promotes amyloid-beta degredation and GSK-3 phosphorylation via a metal chaperone activity. J. Neurochem 2011, 119 (1), 220–230. [PubMed: 21797865]

(24). White AR; Du T; Laughton KM; Volitakis I; Sharples RA; Xilinas ME; Hoke DE; Holsinger RMD; Evin G; Cherny RA; Hill AF; Barnham KJ; Li Q-X; Bush AI; Masters CL Degradation of

the Alzheimer disease amyloid β-peptide by metal-dependent up-regulation of metalloprotease activity. J. Biol. Chem 2006, 281, 17670–17680. [PubMed: 16648635]

(25). Pushie MJ; Nienaber KH; Summers KL; Cotelesage JJH; Ponomarenko O; Nichol HK; Pickering IJ; George GN The solution structure of the copper clioquinol complex. J. Inorg. Biochem 2014, 133, 50–56. [PubMed: 24503514]

(26). Summers KL; Pushie MJ; Sopasis GJ; James AK; Dolgova NV; Kroll T; Sokaras D; Harris HH; Pickering IJ; George GN Solution chemistry of copper(II) binding to 8-hydroxyquinolines. Inorg. Chem 2020, 59 (19), 13858–13874. [PubMed: 32936627]

(27). Kenche VB; Zawisza I; Masters CL; Bal W; Barnham KJ; Drew SC Mixed ligand Cu^{2+} complexes of a model therapeutic with Alzheimer's amyloid-β peptide and monoamine neurotransmitters. Inorg. Chem 2013, 52, 4303–4318. [PubMed: 23537393]

(28). Liu Y-C; Wei J-H; Chen Z-F; Liu M; Gu Y-Q; Huang K-B; Li Z-Q; Liang H The antitumor activity of zinc(II) and copper(II) complexes with 5,7-dihalo-substituted-8-quinolinoline. Eur. J. Med. Chem 2013, 69, 554–563. [PubMed: 24095749]

(29). Nguyen M; Vendier L; Stigliani J-L; Meunier B; Robert A Structures of the copper and zinc complexes of PBT2, a chelating agent evaluated as potential drug for neurodegenerative diseases. Eur. J. Inorg. Chem 2017, 2017 (2017), 600–608.

(30). Di Vaira M; Bazzicalupi C; Orioli P; Messori L; Bruni B; Zatta P Clioquinol, a drug for Alzheimer's disease specifically interfering with brain metal metabolism: Structural characterization of its zinc(II) and copper(II) complexes. Inorg. Chem 2004, 43, 3795–3797. [PubMed: 15206857]

(31). Tardito S; Barilli A; Bassanetti I; Tegoni M; Bussolati O; Franchi-Gazzola R; Mucchino C; Marchio L Copper-dependent cytotoxicity of 8-hydroxyquinoline derivatives correlates with their hydrophobicity and does not require caspase activation. J. Med. Chem 2012, 55, 10448–10459. [PubMed: 23170953]

(32). Sgarlata C; Arena G; Bonomo RP; Giuffrida A; Tabbi G Simple and mixed complexes of copper(II) with 8-hydroxyquinoline derivatives and amino acids: Characterization in solution and potential biological implications. J. Inorg. Biochem 2018, 180, 89–100. [PubMed: 29247871]

(33). Albert A; Gibson MI; Rubbo SD The influence of chemical constitution on anti-bacterial activity. Part VI: The bactericidal action of 8-hydroxyquinoline (oxine). Br. J. Exp. Pathol 1953, 34 (2), 119–130. [PubMed: 13051519]

(34). Hollingshead RGW Oxine; Butterworths Scientific Publications: London, 1954; Vol. I.

(35). Budimir A; Humbert N; Elhabiri M; Osinska I; Biruć M; Albrecht-Gary A-M Hydroxyquinoline based binders: Promising ligands for chemotherapy. J. Inorg. Biochem 2011, 105 (3), 490–496. [PubMed: 20926137]

(36). Welcher FJ Quinoline and quinoline derivatives. In Organic Analytical Reagents; D. Van Nostrand Company, Inc.: 1947; Vol. 3, p 49.

(37). Phillips JP The reactions of 8-quinolinol. Chem. Rev 1956, 56 (2), 271–297.

(38). Nienaber KH; Jake PM; Cotelesage JJH; Pickering IJ; George GN Cryoprotectants severely exacerbate X-ray-induced photoreduction. J. Phys. Chem. Lett 2018, 9, 540–544. [PubMed: 29337573]

(39). Peisach J; Blumberg WE Structural implications derived from the analysis of electron paramagnetic resonance spectra of natural and artificial copper proteins. Arch. Biochem. Biophys 1974, 165, 691–708. [PubMed: 4374138]

(40). Summers KL; Schilling KM; Roseman G; Markham KA; Dolgova NV; Kroll T; Sokaras D; Millhauser GL; Pickering IJ; George GN X-ray absorption spectroscopy investigations of copper(II) coordination in the human amyloid β peptide. Inorg. Chem 2019, 58 (9), 6294–6311. [PubMed: 31013069]

(41). Henthorn JT; Arias RJ; Koroidov S; Kroll T; Sokaras D; Bergmann U; Rees DC; DeBeer S Localized Electronic Structure of Nitrogenase FeMoco Revealed by Selenium K-Edge High Resolution X-ray Absorption Spectroscopy. J. Am. Chem. Soc 2019, 141 (34), 13676–13688. [PubMed: 31356071]

(42). Castillo RG; Banerjee R; Allpress CJ; Rohde GT; Bill E; Que L; Lipscomb JD; DeBeer S High-Energy-Resolution Fluorescence-Detected X-ray Absorption of the Q Intermediate of Soluble

Methane Monooxygenase. J. Am. Chem. Soc 2017, 139 (49), 18024–18033. [PubMed: 29136468]

(43). Cutsail GE; Banerjee R; Zhou A; Que L; Lipscomb JD; DeBeer S High-Resolution Extended X-ray Absorption Fine Structure Analysis Provides Evidence for a Longer Fe···Fe Distance in the Q Intermediate of Methane Monooxygenase. J. Am. Chem. Soc 2018, 140 (48), 16807–16820. [PubMed: 30398343]

(44). James AK; Nehzati S; Dolgova NV; Sokaras D; Kroll T; Eto K; O'Donoghue JL; Watson GE; Myers GJ; Krone PH; Pickering IJ; George GN Rethinking the Minamata Tragedy: What Mercury Species Was Really Responsible? Environ. Sci. Technol 2020, 54 (5), 2726–2733. [PubMed: 31951385]

(45). Teo BK EXAFS: Basic Principles and Data Analysis; Springer-Verlag: Berlin, Germany, 1986; Vol. 9, p 349.

(46). Glatzel P; Bergmann U High resolution 1s core hole X-ray spectroscopy in 3d transition metal complexes - electronic and structural information. Coord. Chem. Rev 2005, 249, 65–95.

(47). Bissardon C; Proux O; Bureau S; Suess E; Winkel LHE; Conlan RS; Francis LW; Khan IM; Charlet L; Hazemann JL; Bohic S Sub-ppm level high energy resolution fluorescence detected X-ray absorption spectroscopy of selenium in articular cartilage. Analyst 2019, 144 (11), 3488–3493. [PubMed: 30939183]

(48). Kosugi N; Yokoyama T; Asakura K; Kuroda H Polarized Cu K-edge XANES of square planar $CuCl4^{2-}$ ion. Experimental and theoretical evidence for shake-down phenomena. Chem. Phys 1984, 91 (2), 249–256.

(49). Yokoyama T; Kosugi N; Kuroda H Polarized XANES spectra of $CuCl_2.H_2O$. Further evidence for shake-down phenomena. Chem. Phys 1986, 103, 101–109.

(50). Pickering IJ; George GN Polarized X-ray absorption spectroscopy of cupric chloride dihydrate. Inorg. Chem 1995, 34 (12), 3142–3152.

(51). Stevenson RL; Freiser H Tridentate ligands derived from substitution in the methyl group of 8-hydroxyquinaldine. Anal. Chem 1967, 39 (12), 1354–1358.

(52). Johnston WD; Freiser H Structure and behavior of organic analytical reagents. III. Stability of chelates of 8-hydroxyquinoline and analogous reagents. J. Am. Chem. Soc 1952, 74 (21), 5239–5242.

(53). Gupta RD; Manku GS; Bhat AN; Jain BD Determination and comparison of the stability constants of some bivalent ion complexes of 5,7-dichloro-, 5,7-dibromo-, and 5,7-dinitro-8-hydroxyquinoline and their N-oxides. Z. Anorg. Allg. Chem 1971, 379, 312–319.

(54). Mital M; Zawisza I; Wiloch MZ; Wawrzyniak UE; Kenche VB; Wróblewski W; Bal W; Drew SC Copper exchange and redox activity of a prototypical 8-hydroxyquinoline: Implications for therapeutic chelation. Inorg. Chem 2016, 55, 7317–7319. [PubMed: 27409140]

(55). Ceolin J; Siqueira JD; Martins FM; Piquini PC; Iglesias BA; Back DF; Manzoni de Oliveira G Oxazolidine copper complexes: Synthesis, characterization and superoxide dismutase activity of copper(II) complexes with oxazolidine ligands derived from hydroxyquinoline carboxaldehyde. Appl. Organomet. Chem 2018, 32 (4), No. e4218.

(56). Hickey JL; Crouch PJ; Mey S; Caragounis A; White JM; White AR; Donnelly PS Copper(II) complexes of hybrid hydroxyquinoline-thiosemicarbazone ligands: GSK3β inhibition due to intracellular delivery of copper. Dalton T. 2011, 40 (6), 1338–1347.

(57). Petkova EG; Domasevitch KV; Gorichko MV; Zub VY; Lampeka RD New coordination compounds derived from nitrone ligands: Copper(II) complexes with 8-hydroxyquinoline-2-carbaldehyde- and pyridine-2-carbaldehyde-N-methylnitrones. Z. Naturforsch., B: J. Chem. Sci 2001, 56 (12), 1264.

(58). Okuniewski A; Rosiak D; Chojnacki J; Becker B Coordination polymers and molecular structures among complexes of mercury(II) halides with selected 1-benzoylthioureas. Polyhedron 2015, 90, 47–57.

(59). Yang L; Powell DR; Houser RP Structural variation in copper(I) complexes with pyridylmethylamide ligands: Structural analysis with a new four-coordinate geometry index, $\tau 4$. Dalton T 2007, No. 9, 955–964.

(60). Sousa SF; Fernandes A; Ramos MJ General performance of density functionals. J. Phys. Chem. A 2007, 111, 10439–10452. [PubMed: 17718548]

(61). George GN EXAFSPAK; https://www-ssrl.slac.stanford.edu/~george/exafspak/exafs.htm, 2001.

(62). Lech T; Sadlik JK Copper concentration in body tissues and fluids in normal subjects of southern Poland. Biol. Trace Elem. Res 2007, 118 (1), 10–15. [PubMed: 17848725]

(63). Lovell MA; Robertson JD; Teesdale WJ; Campbell JL; Markesbery WR Copper, iron and zinc in Alzheimer's disease senile plaques. J. Neurol. Sci 1998, 158, 47–52. [PubMed: 9667777]

(64). Barnham KJ; Gautier ECL; Kok GB; Krippner G Preparation of 8-hydroxyquinolines for treatment of neurological conditions. 2008. U.S. Pat. Appl. Publ Patent version number 20080161353 A1, United States.

(65). Nehzati S; Dolgova NV; Sokaras D; Kroll T; Cotelesage JJH; Pickering IJ; George GN A photochemically generated selenyl free radical observed by high energy resolution fluorescence detected X-ray absorption spectroscopy. Inorg. Chem 2018, 57 (17), 10867–10872. [PubMed: 30133265]

(66). Sokaras D; Weng T-C; Nordlund D; Alonso-Mori R; Velikov P; Wenger D; Garachtchenko A; George M; Borzenets V; Johnson B; Rabedeau T; Bergmann U A seven-crystal Johann-type hard X-ray spectrometer at the Stanford Synchrotron Radiation Lightsource. Rev. Sci. Instrum 2013, 84, 053102. [PubMed: 23742527]

(67). George GN; Pickering IJ; Jake PM; Nienaber KH; Hackett MJ; Ascone I; Hedman B; Hodgson KO; Aitken JB; Levina A; Glover C; Lay PA X-ray-induced photo-chemistry and X-ray absorption spectroscopy of biological samples. J. Synchrotron Radiat 2012, 19, 875–886. [PubMed: 23093745]

(68). George GN; Garrett RM; Prince RC; Rajagopalan KV The molybdenum site of sulfite oxidase: A comparison of wildtype and the cysteine 207 to serine mutant using X-ray absorption spectroscopy. J. Am. Chem. Soc 1996, 118, 8588–8592.

(69). George MJ XAS-Collect: A computer program for X-ray absorption spectroscopic data acquisition. J. Synchrotron Radiat 2000, 7 (4), 283–286. [PubMed: 16609209]

(70). Patton D; Pederson M; Porezag D The Generalized-Gradient Approximation to density functional theory and bonding. In Frontiers in Materials Modelling and Design; Kumar V, Sengupta S, Raj B, Eds.; Springer: Berlin, 1998; pp 37–50.

(71). Perdew JP; Burke K; Ernzerhof M Generalized Gradient Approximation made simple. Phys. Rev. Lett 1996, 77 (18), 3865–3868. [PubMed: 10062328]

(72). Tao J; Perdew JP; Staroverov VN; Scuseria GE Climbing the density functional ladder: Nonempirical meta-Generalized Gradient Approximation designed for molecules and solids. Phys. Rev. Lett 2003, 91 (14), 146401. [PubMed: 14611541]

(73). Peverati R; Truhlar DG M11-L: A local density functional that provides improved accuracy for electronic structure calculations in chemistry and physics. J. Phys. Chem. Lett 2012, 3 (1), 117–124.

(74). Nilges MJ Electron paramagnetic resonance studies of low symmetry nickel(I) and molybdenum(V) complexes. Ph.D. dissertation. University of Illinois: Urbana, IL, 1979.

(75). Maurice AM Acquisition of anisotropic information by computational analysis of isotropic EPR spectra. Ph.D. dissertation. University of Illinois: Urbana, IL, 1980.

(76). Mustre de Leon J; Rehr JJ; Zabinsky SI; Albers RC *Ab initio* curved-wave X-ray-absorption fine structure. Phys. Rev. B: Condens. Matter Mater. Phys 1991, 44 (9), 4146–4156.

(77). Rehr JJ; Mustre de Leon J; Zabinsky SI; Albers RC Theoretical X-ray absorption fine structure standards. J. Am. Chem. Soc 1991, 113 (14), 5135–5140.

(78). Pushie MJ; Cotelesage JJH; Lyashenko G; Hille R; George GN X-ray absorption spectroscopy of a quantitatively Mo(V) dimethyl sulfoxide reductase species. Inorg. Chem 2013, 52 (6), 2830–2837. [PubMed: 23445435]

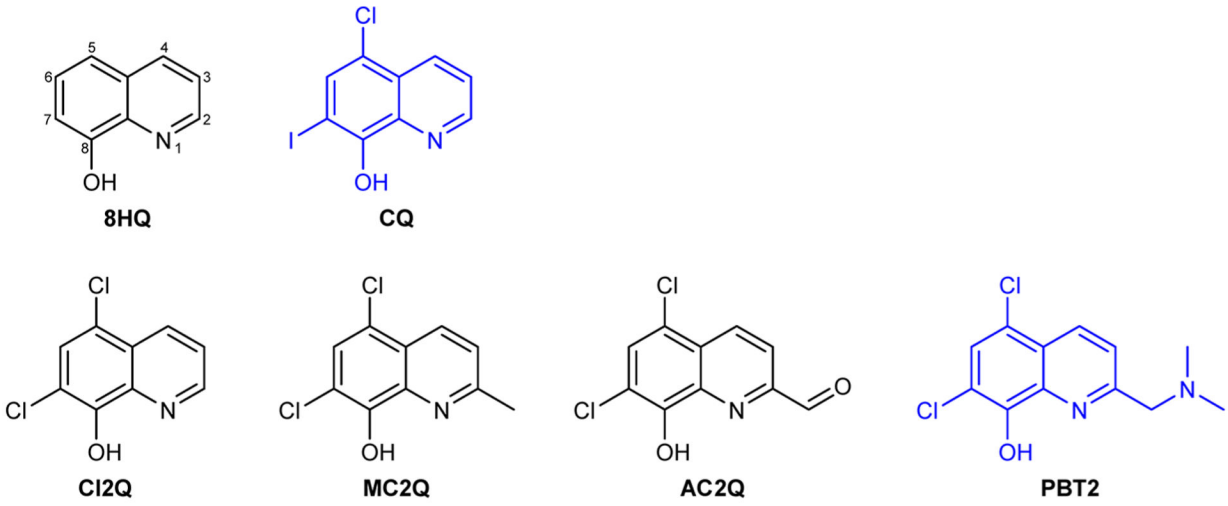

Figure 1.

Schematic structures of 8-hydroxyquinoline (showing ring numbering) and 8-hydroxyquinoline derivative compounds tested as anti-Alzheimer's disease compounds (blue), and/or compared herein. See the text for complete chemical names and details.

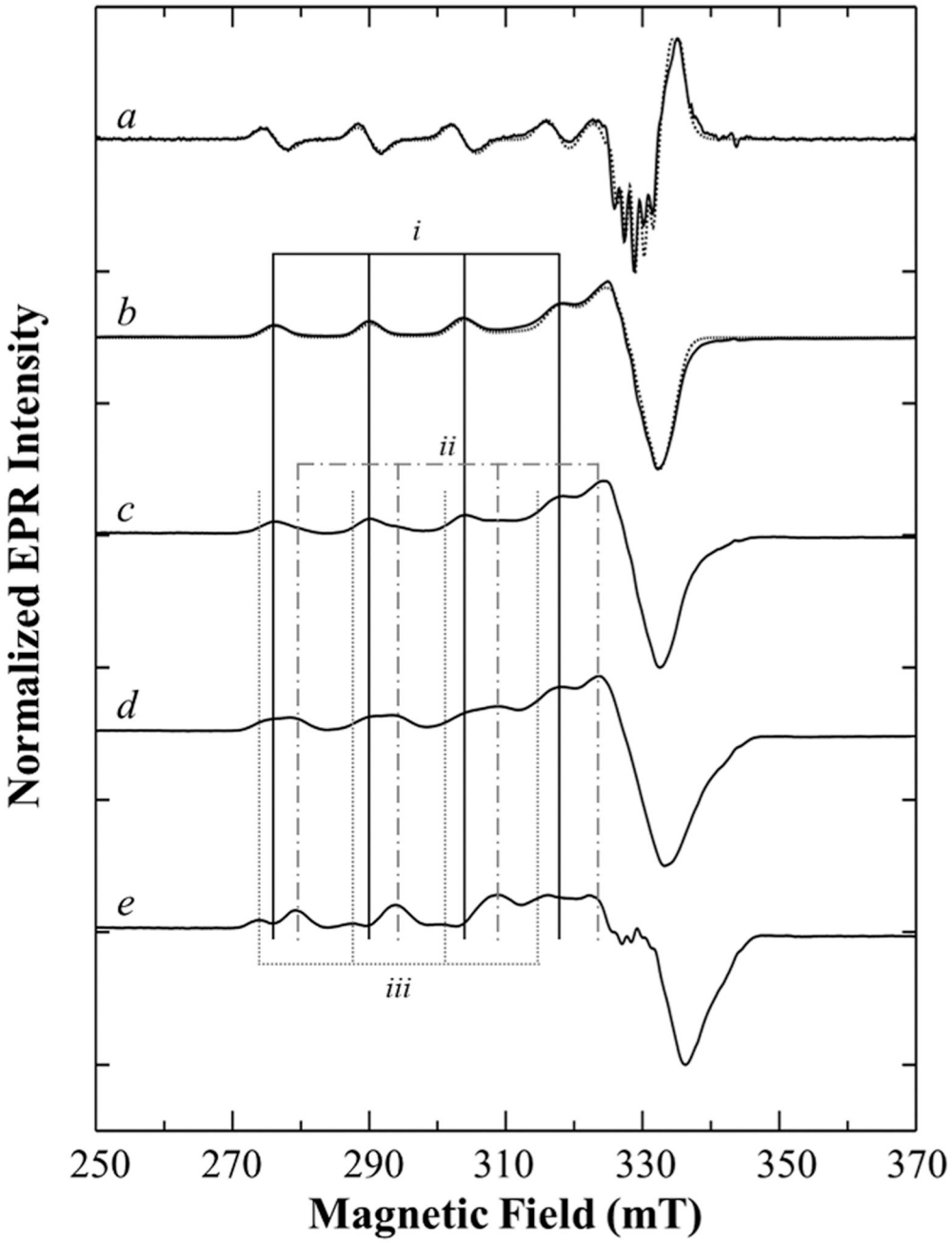

Figure 2.

EPR spectra of ^{63}Cu(II) PBT2 in frozen aqueous solutions. First derivative spectra are shown for solutions with ^{63}Cu(II)/PBT2 ratios of (b) 1:20, (c) 1:2, and (d) 1:1. The second derivative spectrum of (b) is shown in (a). The best simulated spectra of (a) and (b) are overlaid as dashed lines (parameters listed in Table 1). The spectrum shown in (e) is the difference spectrum generated by the subtraction of (b) from (d). The three potential species are indicated by vertical lines and labeled *i* (solid line), *ii* (dashed), and *iii* (dotted). The ^{63}Cu(II) concentration was kept constant at 250 μM; the PBT2 concentration was 5 mM, 500 μM, and 250 μM in b–d, respectively. The buffer used was 400 mM DTAB in 100 mM

MOPS at pH 7.4 with 25% glycerol. Spectra were normalized to 1 on the basis of the highest intensity and were offset vertically for clarity.

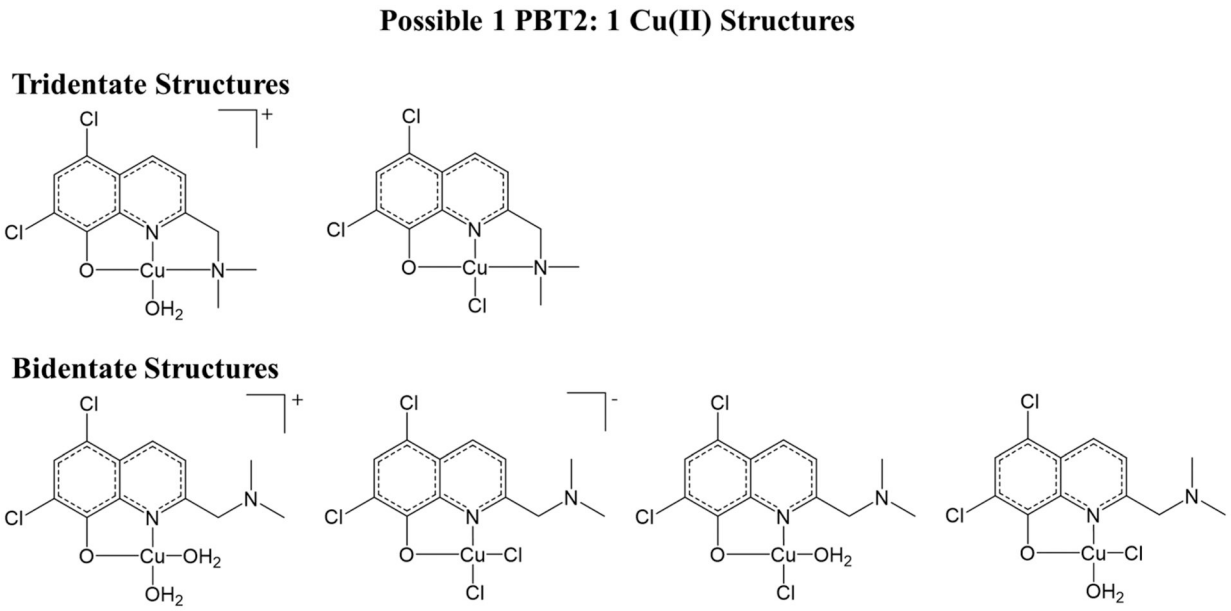

Figure 3.
Possible 1:1 Cu(II)/PBT2 structures that might exist in solution.

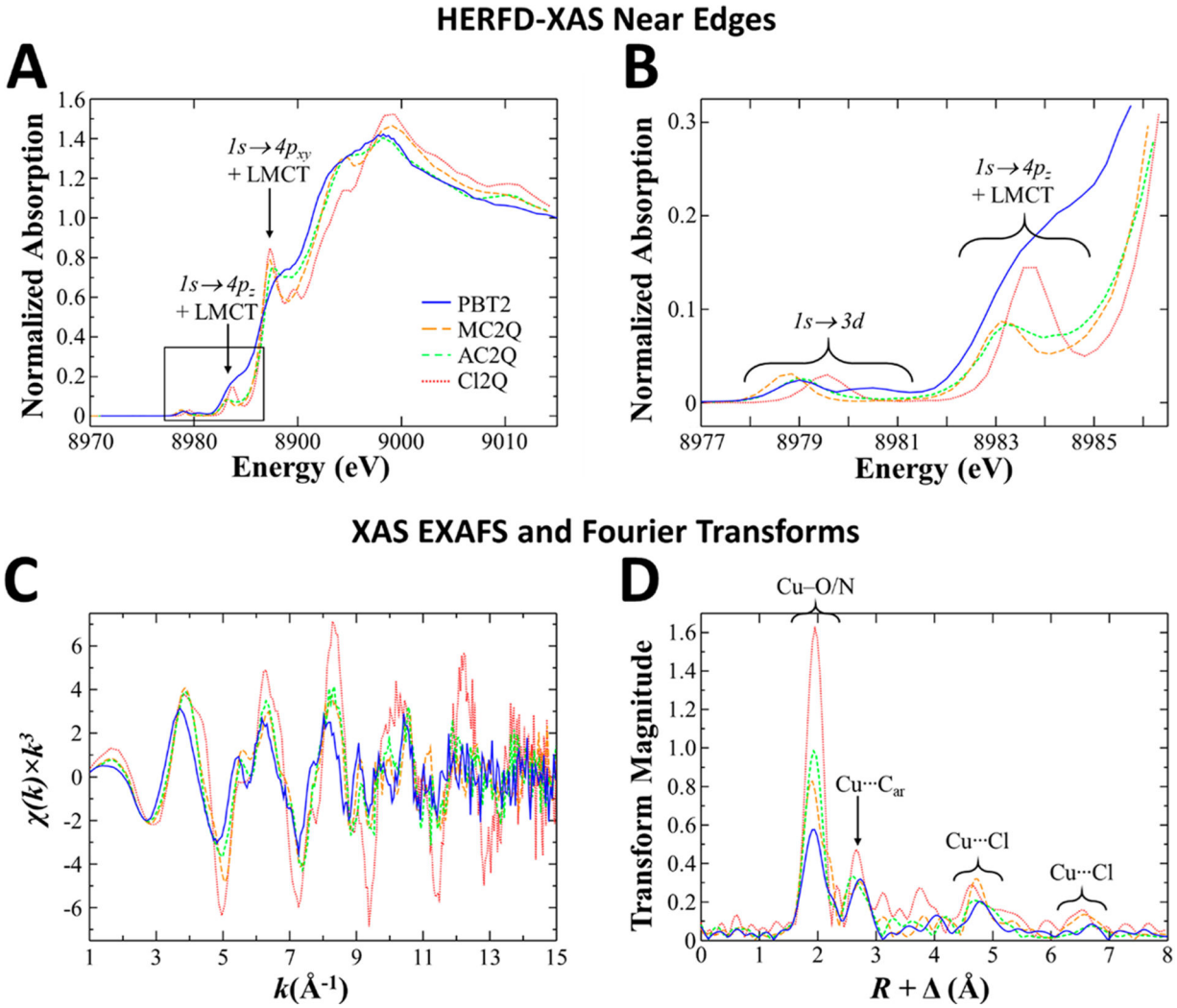

Figure 4.

Comparison of Cu K-edge HERFD-XAS near-edges and conventional XAS EXAFS and Fourier transforms of select 8HQ solution complexes with Cu(II). (A) Cu(II) HERFD-XAS near-edge spectra of Cu(II) complexes of Cl2Q (red), MC2Q (orange), AC2Q (green), and PBT2 (blue). (B) Explanation of near-edge region corresponding to the box in (A) showing select transitions. Note that the 1s → 3d transition is split in spectra of the PBT2 Cu(II) complex. (C) Extended X-ray absorption fine structure (EXAFS) spectra and (D) corresponding Fourier transforms of the conventional XAS data. Solution samples contained 2 mM Cu(II) and 5 mM 8HQ in a mixture of 400 mM DTAB and 100 mM MOPS at pH 7.4. These concentrations were driven by the solubility of the complexes and the detection limits of Cu XAS to allow for sample translation after each energy sweep. Fourier transforms are phase-corrected for Cu–N backscattering.

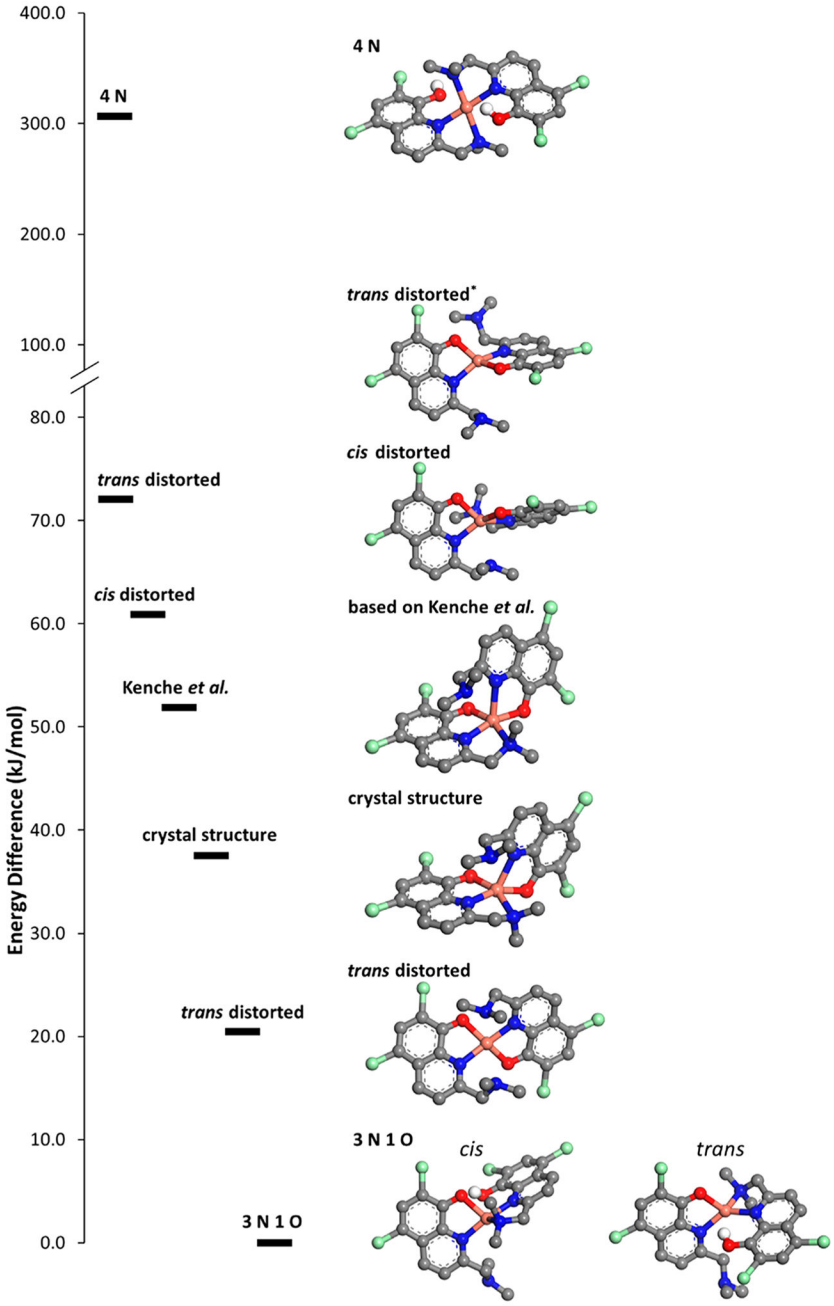

Figure 5.

DFT-geometry-optimized structures of Cu(II) complexes with PBT2. Structures are arranged according to their energy difference, relative to the lowest-energy 3 N 1 O structures, and are indicated by horizontal bars. Note the break in the *y*-axis scale. A conventional color scheme was chosen for each element such that hydrogen is white, carbon is gray, nitrogen is blue, oxygen is red, copper is pink, and chlorine is green.

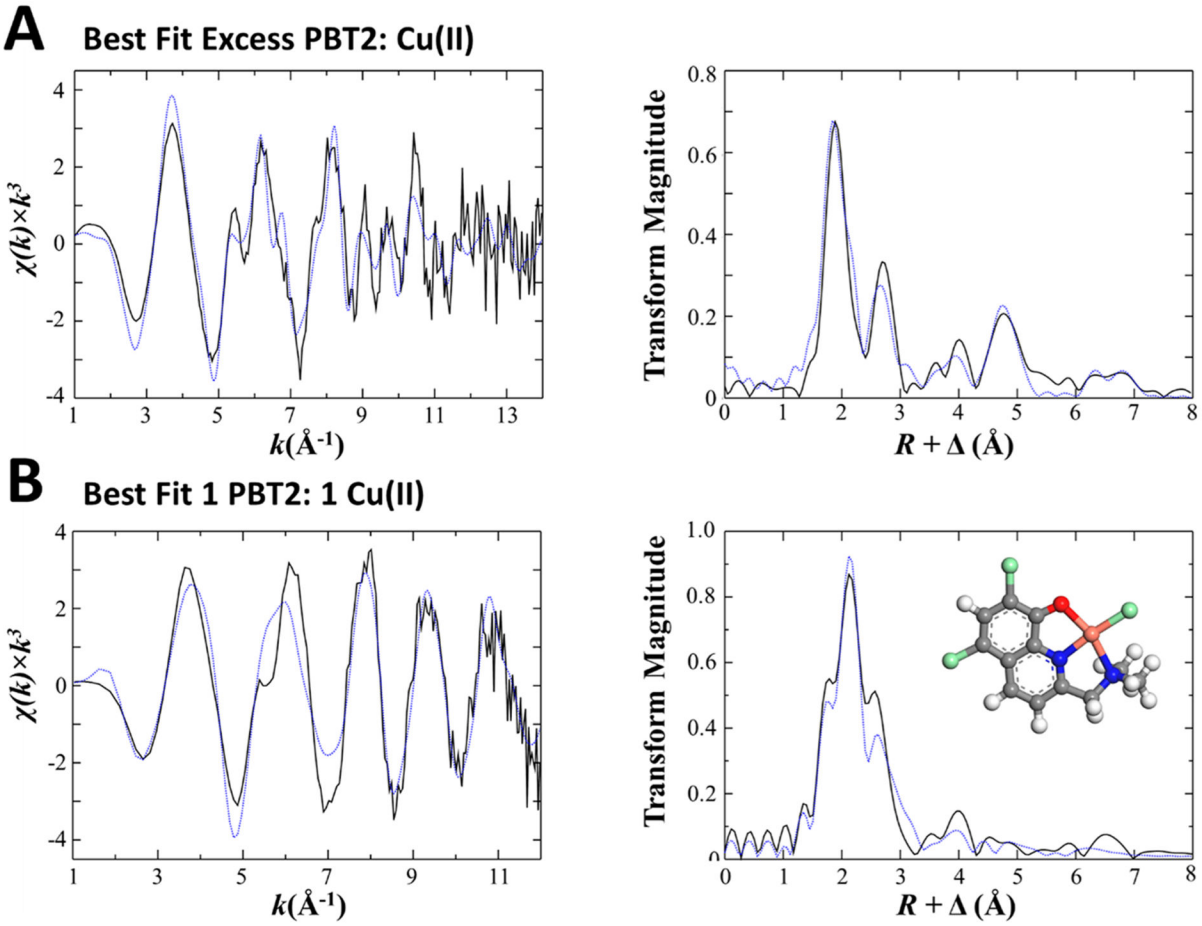

Figure 6.

Cu K-edge EXAFS and Fourier transforms of (A) excess 1:1 PBT2/Cu(II) and (B) 1:1 PBT2/Cu(II). Experimental spectra are shown in black, and best fits are shown as dashed blue lines. (A) Best fit for the Cu(II)-*bis*-PBT2 complex with 2 N 2 O Cu(II) coordination as shown in Figure 7D. (B) Best fit for a possible Cu(II)-*mono*-PBT2 structure in which PBT2 acts as a tridentate ligand with an additional Cl^- ligand (inset). The fits are detailed in Table S.4. In both cases, the experimental spectra are likely composed of a mixture of species, and these fits represent the best fit to the average of these species.

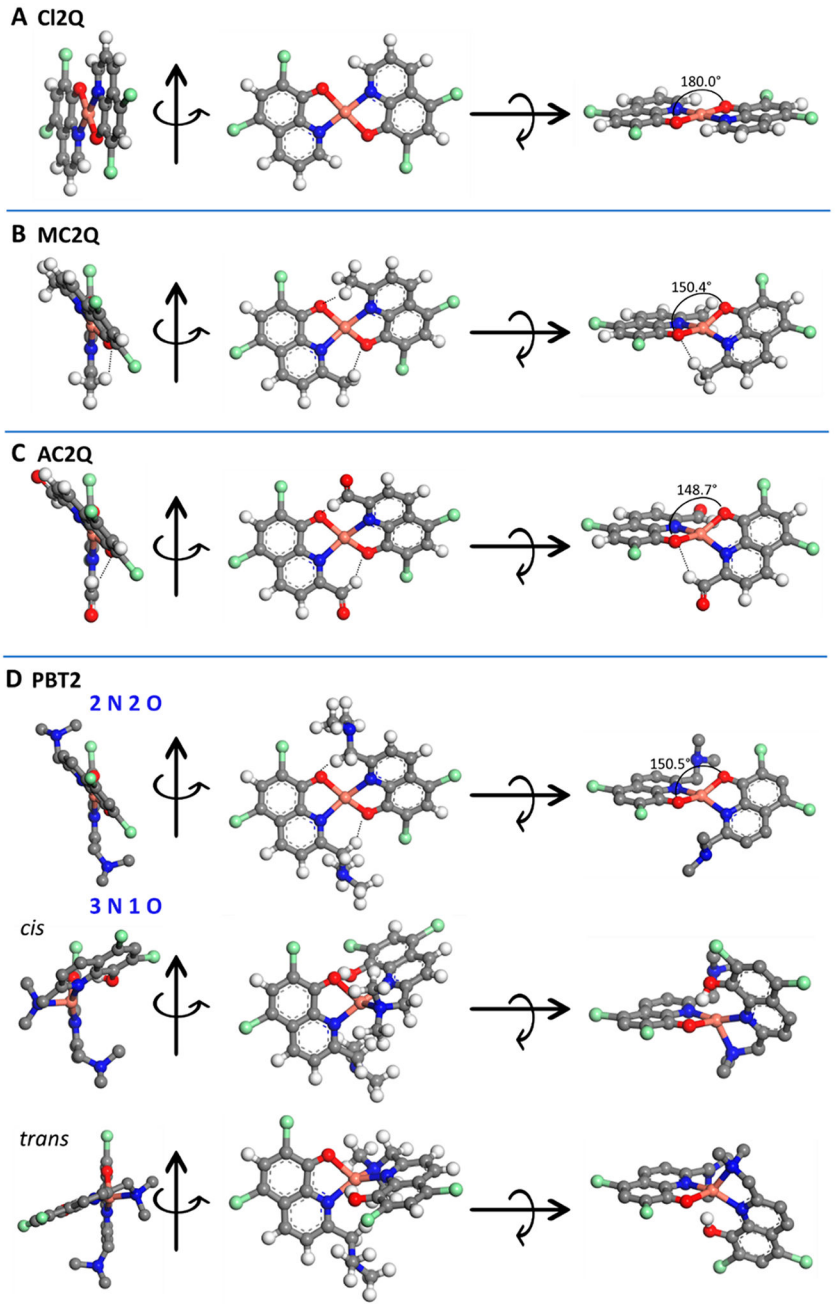

Figure 7.

Geometry-optimized structures for Cu(II) complexes with 5,7-dichloro-8HQs. (A) Cu(II)-*bis*-Cl2Q, (B) Cu(II)-*bis*-MC2Q, (C) Cu(II)-*bis*-AC2Q, and (D) geometry-optimized best-fit structures for Cu(II)-*bis*-PBT2. Different viewpoints of the proposed best fit structures for Cu(II)-*bis*-PBT2 used in the EXAFS fits in Figure 6 and Table S.4 are shown. While included in geometry optimization calculations, hydrogens were omitted in side-on images of PBT2 for clarity. A conventional color scheme was chosen for each element, such that carbon is gray, nitrogen is blue, oxygen is red, copper is pink, and chlorine is green.

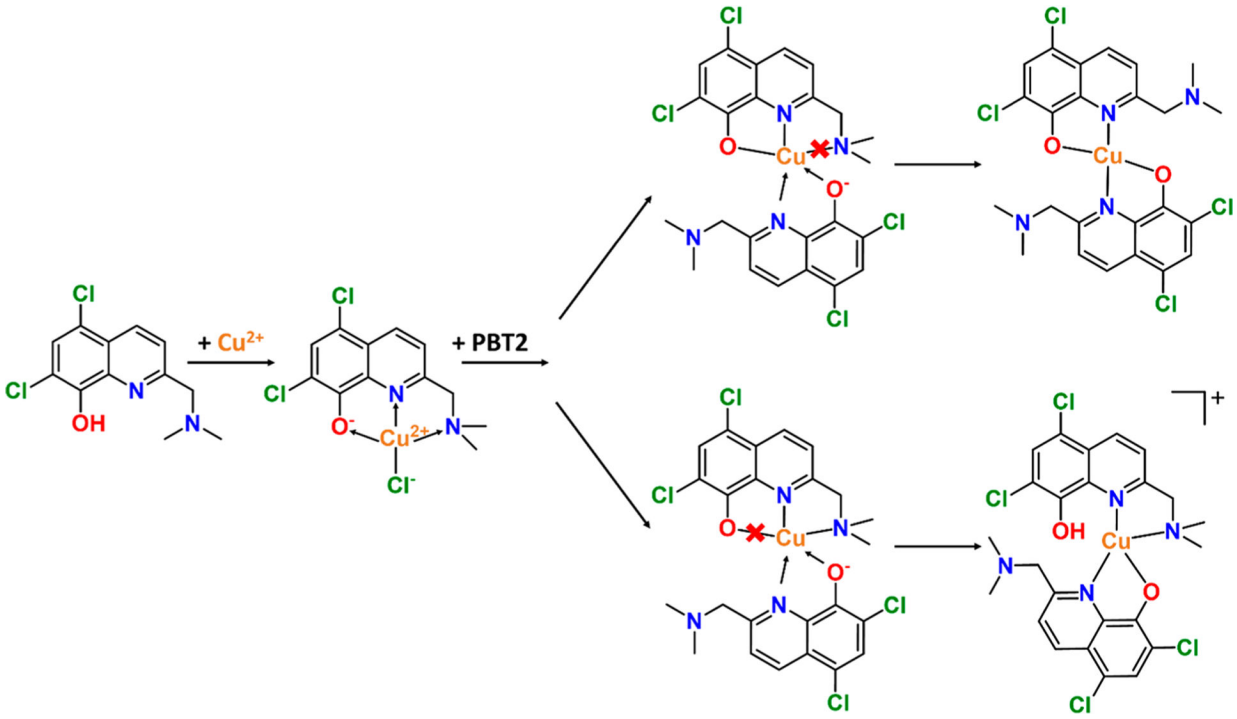

Figure 8.

Schematic diagram for the formation of the energetically favorable Cu(II)-*bis*-PBT2 complexes. Although only the *trans* conformation is shown for the 3 N 1 O complex for simplicity, the *cis* conformation was found to be equally favorable. Overall charges are indicated where the complex that is formed is not neutral.

Table 1.

EPR Parameters for PBT2 Complexes with Copper(II)[a]

Cu(II) complex	solution conditions	$g_{\parallel}$	$g_{\perp}$		$A_{\parallel}$ (mHz)	$A_{\perp}$ (mHz)		ref
			g_x	g_y		A_x	A_y	
1:1 L[b]/ Cu(II)	1% DMSO	2.255	2.055		459			Kenche et al.[27]
2:1 L[b]/Cu(II)	1% DMSO	2.267	2.061		447			Kenche et al.[27]
1:1 PBT2/ Cu(II)	DMSO	2.269			453			Nguyen et al.[29]
2:1 PBT2/ Cu(II)	DMSO	2.275			417			Nguyen et al.[29]
$[Cu(PBT2)]^+$	aqueous solution, pH 6.5	2.261			450			Sgarlata et al.[32]
$Cu(PBT2)_2$	aqueous solution, pH 6.5	2.208			423			Sgarlata et al.[32]
Cu(II)-*bis*-PBT2[c]	**DTAB and MOPS, pH 7.4**	**2.271**	**2.060**	**2.052**	**438**	**20**	**30**	**this work**

[a] Values determined in this study are shown in bold.

[b] L = 2-[(dimethylamino)methyl]-8-hydroxyquinoline.

[c] Measured from the 1:20 Cu(II)/PBT2 spectrum shown in Figure 2b and its derivative shown in Figure 2a.

Table 2.

HERFD-XAS Near-Edge Transition Energies and Intensities in the Cu K Edge of Select Cu(II)-*bis*-8HQ Complexes with 5,7-Dichlorinated 8HQs[a]

	1s → 3d energy	1s → 3d intensity	1s → 3d′ energy	1s → 3d′ intensity	1s → $4p_z$ energy	1s → $4p_z$ intensity	1s → $4p_{xy}$ energy	1s → $4p_{xy}$ intensity	two-position substitution
Cl2Q	8979.5	0.029			8983.7	0.144	8987.3	0.84	none
MC2Q	8978.7	0.030			8983.1	0.088	8987.3	0.78	$-CH_3$
AC2Q	8979.0	0.026			8983.2	0.085	8987.6	0.75	−CHO
PBT2	8979.0	0.024	8980.4	0.016	8983.9	0.183	8988.2	0.71	$-CH_2N(CH_3)_2$

[a]Intensity was measured as the maximum point on each peak of the experimental HERFD-XAS near-edge spectra. Energies are in electron volts (eV).

Table 3.

Stability Constants of 2-Position-Substituted 8HQs from the Literature

8HQ	log K_1	log K_2	2-position substituent	tridentate coordination[a]	ref
8HQ	13.49	12.73	−H	N	Johnston and Freiser[52]
8HQ	13.29	12.61	−H	N	Stevenson and Freiser[51]
CQ	12.50	10.90	−H	N	Budimir et al.[35]
Cl2Q	11.78	12.01	−H	N	Gupta et al.[53]
2-methyl-8HQ	13.00	11.64	$-CH_3$	N	Johnston and Freiser[52]
2-methyl-8HQ	11.92	10.90	$-CH_3$	N	Stevenson and Freiser[51]
8-quinolinol-2-carboxaldehyde oxime	>9		−CHNOH	N	Stevenson and Freiser[51]
2-hydroxymethyl-8-quinolinol	>9		$-CH_2OH$	N	Stevenson and Freiser[51]
2-aminomethyl-8-quinolinol	15.90	8.00	$-CH_2NH_2$	Y	Stevenson and Freiser[51]
2-[(dimethylamino)-methyl-8-hydroxyquinoline	10.44	4.54	$-CH_2N(CH_3)_2$	Y	Mital et al.[54]
PBT2	13.61	5.95	$-CH_2N(CH_3)_2$	Y	Sgarlata et al.[32]

[a]Tridentate coordination proposed for the Cu(II)-*mono*-8HQ complex based on the stability constants.